SANDRA
D6.2.3 - REPORT ON LONG TERM AEROMACS EVOLUTION

Document Manager:	Paola Pulini	DLR	Editor

Programme:	Seamless Aeronautical Networking Through Integration of Data Links, Radios and Antennas
Project Acronym:	SANDRA
Contract Number:	FP7-AAT-2008-RTD-1 – Grant Agreement 233679
Project Coordinator:	SELEX ELSAG
SP Leader:	SEL

Document Id N°:	SANDRA_D6.2.3_20120928_v1.1	**Version:**	v1.1
Deliverable:	D6.2.3	**Date:**	28/09/2012
		Status:	Approved

Document classification	**PUblic**

Approval Status	
Prepared by:	Paola Pulini – DLR
Approved by (WP Leader) :	Paola Pulini – DLR
Approved by (SP Leader) :	Roberto Agrone – SEL
Approved by (Coordinator) :	Paolo Di Michele – SEL

CONTRIBUTING PARTNERS

Name	Company / Organization	Role / Title
Paola Pulini	DLR	Editor
Lorenzo Tapponecco	UPI	Author
Luca Sanguinetti	UPI	Author
Thomas Gräupl	USBG	Author
Michele Conti	UPI	Author
Dario Petri	UPI	Author/Reviewer
Amerigo Capria	UPI	Reviewer
Enzo Dalle Mese	UPI	Reviewer

DISTRIBUTION LIST

Name	Company / Organization	Role / Title
Stephanie Stoltz-Douchet	EC DG RTD	EC Programme Officer
Hans Josef von den Driesch	EC DG RTD	EC Programme Officer
All Company Project Managers	All involved	Members of the Steering Committee

REVISION TABLE

Version	Date	Modified Pages	Modified Sections	Comments
V0.1	26.07.2012	-	All	Document Created
V1.0	20.09.12	All	All	Final Draft V1.0
V1.1	28.09.12	All	All	Final version

CONTENTS

LIST OF TABLES

LIST OF FIGURES

Abbreviations

4D	4 Dimensional
4G	Fourth Generation
A	Austria
ACARE	Advisory Council for Aeronautical Research in Europe
ACARS	Aircraft Communications Addressing and Reporting System
ACC	Area Control Centre
ACG	Austro Control
ACP	Aeronautical Communications Panel
AEA	Association of European Airlines
AFAS	Aircraft in the Future ATM System
AFTM	Air Traffic Flow Management
A/G	Air/Ground
AIS	Aircraft Information Service
AMCP	Aeronautical Mobile Communications Panel
ANS	Air Navigation Services
ANSP	Air Navigation Service Providers
AOC	Airline Operations Centre
APC	Aeronautical Passenger Communications
APP	Approach
ARC	Aeronautical Radio Communications
ARINC	American Radio INCorporation
ASAS	Airborne Separation Assurance System
A-SMGCS	Advanced – Surface Movement Guidance and Control System
ATC	Air Traffic Control
ATIS	Automatic Terminal Information Service
ATM	Air Traffic Management
ATN	Aeronautical Telecommunication Network
ATS	Air Traffic Services
ATSPs	Air Traffic Services Providers
B-VHF	Broadband – VHF
BER	Bit Error Rate
CAA	Civil Aviation Authority
CASCADE	Co-operative ATS through Surveillance and Communication Applications Deployed in ECAC
CDM	Code Division Multiplexing, Collaborative Decision Making
CDMA	Code Division Multiple Access
CNS	Communication, Navigation and Surveillance
COM	Communications
CPDLC	Controller Pilot Data Link Communication
D	Germany
DCL	Departure CLearance
DECT	Digital Enhanced Cordless Telecommunications
DFS	Deutsche Flugsicherung GmbH
DG	Directorate General
DLL	Data Link Layer
DLR	Deutsches Zentrum für Luft- und Raumfahrt e.V.
DME	Distance Measuring Equipment
DQPSK	Differential Quadrature Phase Shift Keying
DSB-AM	Dual Side Band Amplitude Modulation
DSP	Digital Signal Processor
DVB	Digital Video Broadcast
E	Spain
EAD	European AIS Database
EATMP	EUROCONTROL Air Traffic Management Programme
EATMS	European Air Traffic Management System
EC	European Commission

ECAC	European Civil Aviation Conference
EU	European Union
EUROCAE	EURopean Organisation for Civil Aviation Equipment
FAA	Federal Aviation Administration
FCS	Future Communications Study (FAA/EUROCONTROL COOPERATIVE R&D; Action Plan 17)
FP7	Seventh Framework Programme
FRQ	Frequentis GmbH
GB	Great Britain
GE	Germany
GMSK	Gaussian Minimum Shift Keying
GSM	Groupe Spécial Mobile
HDLC	High-level Data Link Control
HF	High Frequency
HLTC	High Level Target Concept
HW	Hardware
I	Italy
IATA	International Air Transport Association
ICAO	International Civil Aviation Organisation
InSpE	Increasing Spectrum Efficiency
IFFT	Inverse Fast Fourier Transform
IFR	Instrument Flight Rules
IPR	Intellectual Property Rights
INCO	International Cooperation
ISO	International Organization for Standardization
LH	Lufthansa
LLC	Logical Link Control
MAC	Medium Access
MC-CDMA	Multi-Carrier Code Division Multiple Access
MF	Medium Frequency
MIMO	Multiple-Input-Multiple-Output
MLS	Microwave Landing System
NASA	National Aeronautics and Space Administration
NATS	National Air Traffic Services (UK)
NEXCOM	NEXt-generation COMmunications system (FAA)
OC	Operational Concept
ODIAC	Operational Development of Initial Air / ground Data Communications
OFDM	Orthogonal Frequency Division Multiplexing
OSI	Open System Interconnection
OTE	OTE S.p.A.
PDC	Pre-Departure Clearance
PHY	PHY layer (OSI model)
PP	Point to Point
QM	Quality Management
QoS	Quality of Service
RF	Radio Frequency
R/T	Radio Telephony
RTCA	Radio Technical Commission for Aeronautics
SARPS	Specification And Recommended Practices
SATCOM	SATellite COMmunication
SCG	Serbia and Montenegro
SHF	Super High Frequency
SID	Standard Instrument Departure
SME	Small and Medium Enterprises
SRA	Strategic Research Agenda
STAR	Standard Instrument Arrival
SWIM	System Wide Information Management
SWP	Sub Work Package

TDD	Time Division Duplex
TDMA	Time Division Multiple Access
TETRA	TErrestrial Trunked RAdio
TFTS	Terrestrial Flight Telecommunications System
TMA	Terminal Manoeuvring Area
TTCN	Tree and Tabular Combined Notation
TWR	ToWeR
UAV	Unmanned Air Vehicle
UHF	Ultra High Frequency
UK	United Kingdom
UML	Unified Modelling Language
UMTS	Universal Mobile Telecommunication System
USBG	University of Salzburg
VDL	VHF Digital Link
VDR	VHF Data link Radio
VHF	Very High Frequency
WBS	Work Breakdown Structure
W-CDMA	Wideband CDMA
WG	Working Group
WP	Work Package

1 Introduction

SANDRA work package 6.2 deals with the design of the AeroMACS waveform profile, and comprises different topics from the physical layer to the higher layer design. The main aims of the WP is the assessment of the WiMAX profile via PHY/MAC/CS layer simulations, the identification of the procedures, functions, algorithms, and parameters tailored to the aeronautical applications. Moreover, if necessary, the assessment of minor/major modifications to the selected profile, in order to adapt it to the aeronautical communications.

The final task of WP 6.2 is dedicated to the long term evolution of AeroMACS, and deals with the investigation of potential extensions, improvements, and general enhancements of the system baseline. We tackle different aspects related to the long term AeroMACS evolution, spanning from investigations on potential enhancements of the protocol and front-end, to studies of potential extensions of the utilize of the system as the use of AeroMACS during different flight phases, and the exploitation of the base stations for positioning applications. The document is organized as follows.

Section 2 provides an analysis of the applicability of AeroMACS to the landing, take-off, and approach aircraft phases. The main aspects of these scenarios are investigated and corresponding channel parameters are provided for the numerical analysis. The performance of the system in the new environments is assessed by computer simulations. Beside the general performance of the system expressed in term of bit error rate, an analysis of the synchronization algorithm is included.

Section 3 is dedicated to an analysis of the potential exploitation of the AeroMACS base stations for target identification and positioning. The radar ambiguity function is defined to estimate the spatial resolution, and the radar coverage of a single system is computed in term of signal-to-noise ratio and spatial resolution.

Section 4 illustrates an investigation on potential enhancements of the system. The use of packet-level coding technique is investigated and flexible irregular repeat accumulate (F-IRA) codes are applied to AeroMACS, illustrating great performance improvement. Moreover, the use of cooperative communications-relay techniques is investigated. Simple single-relay schemes as amplify and forward and decode and forward are applied to AeroMACS, showing an increase of the performance of the system.

Section 5 is dedicated to an analysis of potential improvements of the protocol. An investigation on network re-entry and handover optimization is carried out.

Finally, Section 6 summarizes the main outcomes of the investigations presented in this document and draws some final conclusions.

2 Analysis on the Performance of AeroMACS during the Landing/Take-off/Approach Phases

AeroMACS has been initially developed for surface airport communications. Hence, the parking, apron, and taxi aircraft phases represent the conventional application scenario of the system. In this Section, the potential extension of the link to different aircraft phases is investigated, evaluating the applicability of the system to the take-off, landing, and approach phases. We examine the new scenarios, evaluating the main aspects of these flight phases. A coverage analysis is also included.

The performance of the system is assessed by numerical results obtained by computer simulations. Moreover, a detailed synchronization analysis is performed, as in high speed scenarios it constitutes a particularly critical aspect.

AeroMACS can be used for transmission only when the aircraft is on the ground, therefore, in the following analysis we will focus only on the forward link (FL).

2.1 Analysis of the Channel Scenarios

The landing, take-off, and approach phases [ICAO1] represent the periods following and preceding the phases associated to the airport, and correspond to the critical aircraft transition from the en route (flying) phase to touch down (and vice versa). More in detail, they can be defined as follow.

- The take-off phase corresponds to the period during which the aircraft transfers from an altitude of 0 to one of 35 ft above the runway elevation (or until ger-up selection [ICAO1]).
- The approach phase represent the period spanning from the en route flight phase to the landing phase. It is divided in two sub-phases: an initial approach phase called instrument flight rules, which extends from the initial approach fix to the beginning of the landing flare, and a final approach phase. The last one is called visual flight rules (VFR) and includes the period starting with the beginning of the VFR or from an altitude of 1000 ft above the runway elevation (whichever comes first), and finishing at the beginning of the landing flare.
- Last, the landing phase[1] follows the approach phase and finishes with the aircraft stop.

These phases last from the end of the en route phase to a stopping position on the runway, spanning from an altitude of more than 1000 ft to 0 ft (respect to the runway altitude) and covering the airport surface and locations several meters away from the airport. Hence, the propagation channel varies throughout these phases. Besides, it is convenient to perform link-budget considerations, in order to understand whether the AeroMACS base stations are able to cover the areas relative to the "new" flight phases.

[1] This flight phase includes two sub-phases: the landing flare, which consists in the transition from nose-low to nose-up attitude (starting before landing and ending with the touch down); and landing roll, which starts after touch-down and finishes with the stop of the aircraft.

2.1.1 Coverage Considerations

Before analyzing in detail the new channel scenarios, we estimate the area covered by the AeroMACS base stations. In particular, we focus on the aerial zone, which has not been considered in the previous WP activities. In this case, the free space path loss (FSPL) equation can be used; therefore, the distance d is related to the path loss (PL) by the following equation

$$FSPL\ [dB] = 20\log_{10}(4\pi f_c\, d/c) = 20\log_{10} d + 20\log_{10} f_c - 147.55, \quad (2.1)$$

where f_c represents the carrier frequency (f_c= 5.12 GHz), and c is the speed of light (3 10^8 m/s). The maximum distance d_{max} can be obtained from the maximum path loss allowed by the link budget. Thus, inserting in the previous equation the maximum path loss (PL_{max}) allowed by the link budget, the maximum distance d_{max} is obtained as

$$d_{max} = (PL_{max})^{1/2}\, c/(4\pi f_c) = \quad . \quad (2.2)$$

Using the AeroMACS transmitter and receiver parameters provided in [D612], we obtain the link budgets summarized in Table 1. The maximum path loss values are obtained as

$$PL_{max} = EIRP_{TX} - RSS, \quad (2.3)$$

where RSS indicates the receiver sensitivity and the transmission effective isotropic radiated power (EIRP) is given by

$$EIRP_{TX}\ [dBm] = P_t \text{ per Ant. element [dBm]} + \text{TX Ant. gain (12 dB)} - \text{TX cable loss (3 dB)}. \quad (2.4)$$

Table 1: Link Budget Parameters

Parameters	P_t	Gain	$EIRP_{TX}$	RSS (QPSK,R=1/2)	PL_{max}	d_{max}
Case 1	30 dBm (max)	9 dB	39 dBm	-89.37 dBm	128.37 dB	12.21 km
Case 2	30 dBm (max)	9 dB	39 dBm	-85 dBm	124.37 dB	7.383 km
Case 3	20 dBm (min)	9 dB	29 dBm	-89.37 dBm	118.37 dB	3.861 km

The three rows of the table represent tree different link budgets, corresponding to the following cases. The first one represents the situation where the transmission power is maximal (equivalent to 30 dBm), while the receiver sensitivity is -89.37 dBm (equivalent to the value specified in [D612]). The second case corresponds to a maximal transmission power and a sensitivity of -85 dBm (equivalent to the sensitivity of the antenna that will be used in the SANDRA final trials). Last, the third case represents the configuration with minimal transmission power (20 dBm) and a sensitivity of -89.37 dBm. Consequently, the maximal distance covered by an AeroMACS base station is 12.21 Km.

The airport domain is defined as the area around the airport having a diameter of 10 miles and a height of 5000 ft, equivalent to a diameter of 16090 m, and a height h_A= 1525 m [COCR], as illustrated in the scheme of **Error! Reference source not found.**. Hence, we can assume the airport domain covered[2].

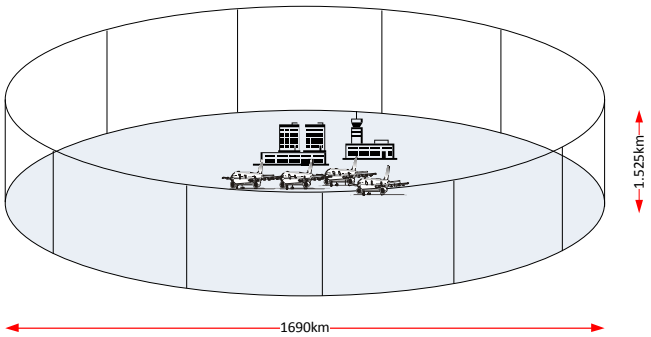

Figure 1: Scheme of the APT Domain

Given the transition nature of these phases, the propagation characteristics largely vary during these periods, spanning over behaviors similar to taxi (when the aircraft is on the runway) and en route scenarios (airborne on the edge of the airport domain).

2.1.2 Channel Scenarios

In order to simplify the channel characterization of the new complex environment composed by the take-off, landing, and approach phases, we approximate it with two different scenarios respectively called runway and landing/take-off airborne. The first one describes the period during which the aircraft is travelling with high speed on the runway (on the ground or with an altitude of few feet). The second scenario represents an airborne situation, with the aircraft at the edge of the airport domain. In the following sections, these scenarios will be described more in detail.

2.1.2.1 *Runway Scenario*

The runway scenario is similar to the taxi one (SANDRA LOS scenario [D621]). In this situation in fact, the aircraft is on the airport surface and is travelling with high speed. On the runway, the aircraft is in line of sight with the control tower. Thus, there is a strong line-of-sight (LOS) path plus some reflected components. We consider the SANDRA channel model still valid. An exponentially decaying power delay profile with delay spread σ_τ=1.05 μs is assumed [GLI09]. The Rice factor (K=12 dB) is high because in this situation we have a strong LOS and fewer reflections with respect to the generic taxi case.

[2] Assuming the base station positioned in the center of the airport domain, the first link budget can provide the coverage of the whole airport domain. However, the airport will have more base stations, offering full coverage of the airport domain also with lower transmit power.

Typical takeoff speeds for jetliners are within the 130–160 knots range (240–285 km/h), while the landing speeds are similar to the takeoff ones, but a bit slower. We consider for this case a takeoff speed of 150 knots (= 277.5 km/h= 77.2 m/s). Therefore, the maximum Doppler shift fd_{max}, given by

$$fd_{max} = f_c * v/c, \quad (2.5)$$

(where f_c= 5.2 GHz is the carrier frequency, v is the speed of the aircraft, and c is the speed of light), is equivalent to 1.32 kHz.

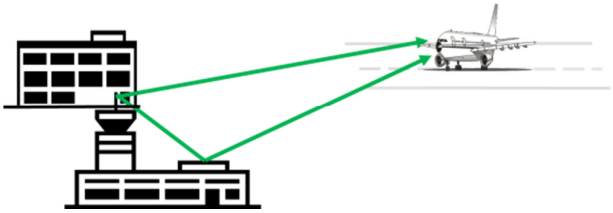

(a) **(b)**

Figure 2: Runway scenario (a), and landing/take-off airborne scenario (b).

2.1.2.2 *Landing/Take-off Airborne Scenario*

This scenario represents an airborne situation, and the propagation condition are similar to the one presented by the en route flying phase. Here, the channel is substantially different from the runway one; in fact, the typical multipath components of the airport surface lacks[3], and we have mainly a strong line-of-sight component. Indeed, we have basically the LOS path plus a reflected one. Hence, we can describe the channel with the geometrical 2-ray model illustrated in Figure 3. Assuming for simplicity the aircraft being in a generic position on the edge of the airport domain (see Figure 2 (b)), we can derive the distances travelled by the two paths and, using a free space propagation model, the relative delays.

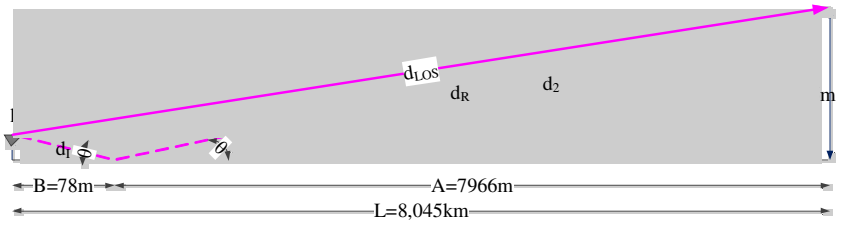

Figure 3: Two paths scheme for the LTA scenario.

The LOS path (indicated by the continuous line) travels a distance d_{LOS}, while the reflected component (represented with a dashed line) travels a distance d_2, obtained summing the distances travelled by the

[3] The aircraft is flying and there are not propagation obstacles.

incident and reflected components. We can obtain the first value as

$$d_{LOS} = \sqrt{\quad\quad}, \qquad (2.6)$$

where h_A and h_T are respectively the heights of control tower and aircraft, while L is the radius of the airport domain (equivalent to the distance between the control tower and the projection point of the aircraft on the ground). The distance travelled by the reflected component is given by

$$d_2 = d_I + d_R = \sqrt{\quad\quad} + \sqrt{\quad\quad} \qquad (2.7)$$

with $d_I=(B^2+h_T^2)^{0.5}$ and $d_I=(A^2+h_A^2)^{0.5}$ being the length of the incident and reflected segments of d_{LOS}. The numerical results are summarized in Table 2. The reflected path d_2 arrives with a fairly small delay with respect to the LOS tap. Therefore, we can assume the two components arriving at the same time (delay $\Delta t = t_2 - t_{LOS} = 0$).

Table 2: 2-ray model parameters

Parameters	**Values**	
h_T	15 m	
h_A	1525 m	
L	8045 m	
A	7966 m	
B	78 m	
$\theta = \arcsin(h_T/l_T)$	0.1891 rad= 10.8346°	
	LOS	**Reflected path**
PL	1.756e+06	1.757e+06
Time of arrival t	27.28 μs	27.3 μs
Δt (= t-t_{LOS})	0	18.62 ns
Distance travelled d [m]	d_{LOS} = 8.185 km	d_2 = 8.191 km
Δd (= d-d_{LOS})	Δd_{LOS} = 0	Δd_2 = 5.587 m

We assume for this scenario the maximum speed allowed in the airport domain, which is equivalent to 200 knots (v_{max}= 102 m/s= 370 Km/h). Hence, the maximum Doppler shift is given by

$$fd_{max} = f_c * v/c = 1.74 \text{ kHz}. \qquad (2.8)$$

Assuming the aircraft travelling in the same direction of the control tower (this is a realistic approximation in the landing case), the Doppler shift of the direct path (line-of-sight) is equivalent to the maximum one $fd_{LOS} = fd_{max}$ (cos $\square_{LOS}$= cos 0= 1). Instead, in case of take-off, $fd_{LOS} = -fd_{max}$.

The Doppler shift of the second (reflected) path may be evaluated from Figure 3 and Figure 4, computing the angle $\Delta\square$ between the two paths (since the first path is assumed equivalent to the direction of travel of the aircraft $\square_2 = \Delta\square$). It results $\Delta\square$ = 0.0489 rad= 2.8°. Hence, the resulting Doppler shift is given by

$$fd_2 = f_c * v/c * \cos \square_2 \approx 0.9988 \approx fd_{max}. \qquad (2.9)$$

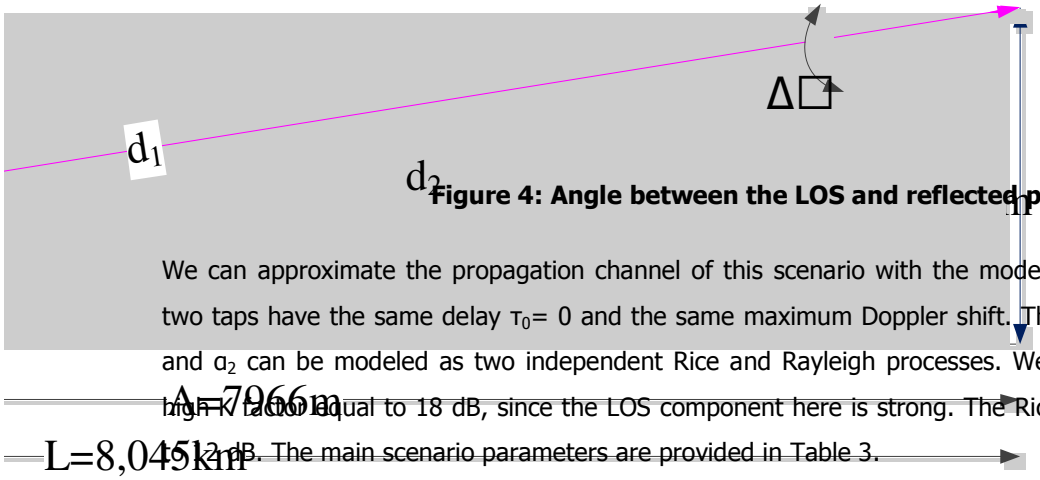

Figure 4: Angle between the LOS and reflected path.

We can approximate the propagation channel of this scenario with the model illustrated in Figure 5. The two taps have the same delay τ_0= 0 and the same maximum Doppler shift. The two fading processes α_{LOS} and α_2 can be modeled as two independent Rice and Rayleigh processes. We assume for this scenario a high K factor equal to 18 dB, since the LOS component here is strong. The Rice factor *R* is assumed equal to 12 dB. The main scenario parameters are provided in Table 3.

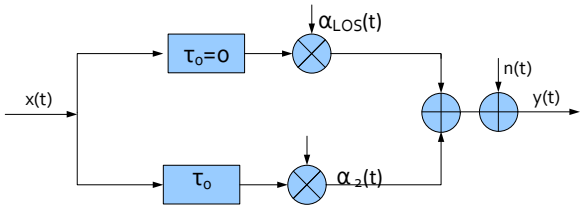

Figure 5: Channel model scheme for the airborne scenario.

2.1.3 Channel Parameters

In this section, we focused on the landing, takeoff, and approach flight phases, considering both the runway area and the airborne edges of the airport domain. In order to characterize the different situations included by these phases, we selected two limit scenarios.

- The runway scenario represents the phase during which the aircraft is still on the airport surface. Here, the propagation conditions are similar to the ones of the taxi phase. We assume still valid the SANDRA channel model. In this phase, we assume a typical speed of 150 knots (= 277.5 km/h= 77.2 m/s), which results in a maximum Doppler shift of 1.31 kHz.

- The second scenario, denominated landing/take-off airborne, has propagation conditions similar to the ones of the en route scenario. In this case, we assume a single LOS path which includes the reflected path. The Doppler shift corresponding to this scenario is equivalent to the maximum one, because we can approximate the direction of the aircraft with the propagation direction.

The following table provides in detail the main channel parameters of the two scenarios. The SANDRA channel model developed in the previous phase of the project [D621] can be used for simulating both these scenarios, provided that the channel parameters are modified according to the new values.

Table 3: Channel parameters for the two scenarios

Parameters	**Values**	
Scenario	**Runway**	**Landing/take-off airborne**
Channel model	SANDRA[4] [D621]	SANDRA[5] [D621]
# Tap	7	2
K [dB]	12	18
R	16	12
PDP/ Tap amplitude	EXP decaying	According to K (c_0~0.99, c_1~0.125)
σ_τ [µs]	1.01	(τ_0= τ_1= 0)
Speed v [m/s]	77.2	102
fd_{max} [kHz]	1.32	1.74
fd	U~[-fd_{max}, fd_{max}]	fd_{max}
θ	U~[0,2π)	U~[0,2π)
Doppler spectrum	Gaussian	Dirac
σ_{fD} [Hz]	between 20 and 100	-
Number of scatterers	25	25

2.2 Bit Error Rate performance

This Section deals with the channel estimation problem in the FL and evaluates the bit-error-rate (BER) performance of the proposed scheme.

2.2.1 Channel Estimation

We begin by recalling that in the AeroMACS standard, there are three types of subcarriers: i) data subcarriers carrying information symbols; ii) pilot subcarriers, carrying known pilots which are exploited for channel estimation and synchronization purposes; iii) null subcarriers, which have no power allocated to them and including DC carriers and guard bands placed at the spectrum edges. In the FL PUSC, the active subcarriers (carrying data or pilot) are divided into physical clusters containing 14 adjacent subcarriers over 2 consecutive OFDMA symbols. In each symbol, 2 subcarriers are allocated for pilots, while the remaining 12 subcarriers are used for data transmission. Figure 6**Error! Reference source not found.** illustrates

[4] The SANDRA channel model can be used for simulating the runway scenario whereas the parameters are set according to the table specifications.

[5] The landing scenario can be obtained from the SANDRA channel model modifying the channel parameters according to the values of Table 3.

the cluster structure and the position of the pilot subcarriers, which is different for even and odd OFDMA symbols.

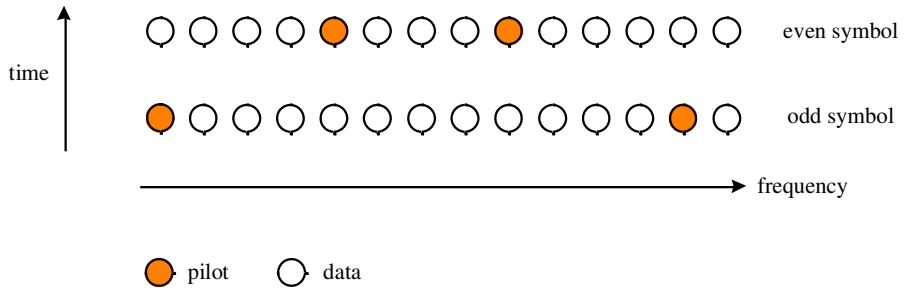

Figure 6: AEROMACS cluster structure in the FL-PUSC

At the receiver side, the incoming samples are converted into the frequency domain through an *N*-point discrete Fourier transform (DFT) operation. Assuming ideal timing and frequency synchronization, the DFT of the k^{th} received symbol takes the form

$$X_k(n) = c_k(n)H_k(n) + w_k(n) \qquad n = 0,1,\ldots,N-1 \tag{2.10}$$

Where $H_k(n)$ is the channel frequency response over the n^{th} subcarrier, $c_k(n)$ is the transmitted (data or pilot) symbol and $w_k(n)$ represents the thermal noise contribution, which is modelled as a white Gaussian process with power σ_w^2. In the FL subframe, the pilots are known BPSK symbols with amplitude 4/3. In practice, the channel response is first estimated at the pilot positions as

$$\hat{H}_m(p) = \frac{X_m(p)}{c_m(p)} \tag{2.11}$$

Where (*m, p*) are the time-frequency coordinates of one of the available pilot tones.

To simplify the notation, we focus on a single cluster and consider two consecutive symbols with time index $k = 0,1$ and frequency index n= 0, 1,… 13. The channel response over the considered cluster is assumed to vary linearly in both the time and frequency directions. This amounts to

$$H_k(n) = ak + bn + c, \tag{2.12}$$

where $\theta = [a,b,c]^T$ are suitable coefficients that must be estimated according to some optimization criterion. Using the least squares (LS) approach yields

$$\hat{a} = \frac{1}{2}\left[-\hat{H}_0(0) + \hat{H}_1(4) + \hat{H}_1(8) - \hat{H}_0(12)\right]$$
$$\hat{b} = \frac{1}{40}\left[-3\hat{H}_0(0) - \hat{H}_1(4) + \hat{H}_1(8) + 3\hat{H}_0(12)\right] \quad (2.13)$$
$$\hat{c} = \frac{1}{20}\left[19\hat{H}_0(0) + 3\hat{H}_1(4) - 3\hat{H}_1(8) + \hat{H}_0(12)\right].$$

The channel estimates over the considered cluster are eventually obtained in the form

$$\hat{H}_k(n) = \hat{a}k + \hat{b}n + \hat{c}, \quad (2.14)$$

with $[\hat{a},\hat{b},\hat{c}]^T$ as given in (2.13). For notational convenience, we refer to (2.13) (2.14) as the 2D channel estimator (2D-CE) in the sequel.

2.2.2 BER results

The performance of the illustrated channel estimation method is assessed by means of numerical analysis. Throughout simulations, we adopt the channel models discussed in Section **Error! Reference source not found.**. The system performance is investigated in terms of BER using 4-QAM and 16-QAM constellation symbols. As specified in [WiM03], we consider a bit-interleaved coded-modulation (BICM) based on the industry-standard convolutional code with rate 1/2 and generator polynomial (131, 171). The FFT size is N=1024, while the number of active subcarriers is 840. The latter are divided into 30 subchannels, which are assigned to the active users. Two boundary cases have been investigated. In the first one, which we denote by scenario#1 (S1), the BS assigns all subchannels to one user. This provides the user with the maximum degree of frequency diversity as its data occupy all the available bandwidth. In the second case, which is referred to as scenario#2 (S2), each user gets only one subchannel and, in consequence, it is expected to suffer from a significant reduction of the diversity gain as compared to S1.

Figure 7 and Figure 8 illustrate the BER for a 4-QAM system as a function of E_b/N_0, where E_b is the average received energy for information bit, while N_0 is the one-sided noise power spectral density. The curve labelled "Ideal" refers to an ideal receiver having perfect knowledge of the channel response over each subcarrier and can be used as a benchmark to the system performance. Compared to Ideal, all the considered schemes entail a loss of approximately 2 dB when the channel is static, which may be interpreted as the loss induced by channel estimation errors.

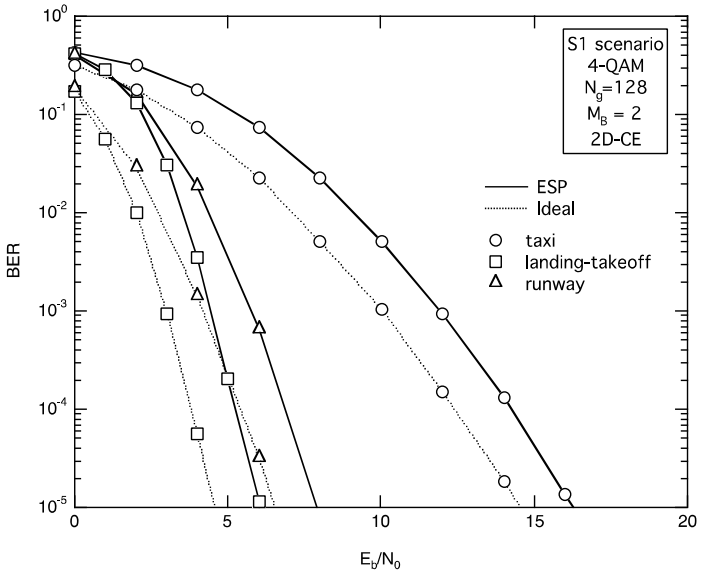

Figure 7: BER for a 4-QAM system endowed with 2D-CE in the FL-S1 scenario.

The best results are obtained with the landing/takeoff channel due to the more favourable conditions. The main difference between the results illustrated in Figure 8 and those illustrated in Figure 7 pertaining to the S1 scenario is that the slope of the BER curves is now significantly reduced, which can be explained by observing that in the S2 case the system cannot exploit all the frequency diversity offered by the propagation channel.

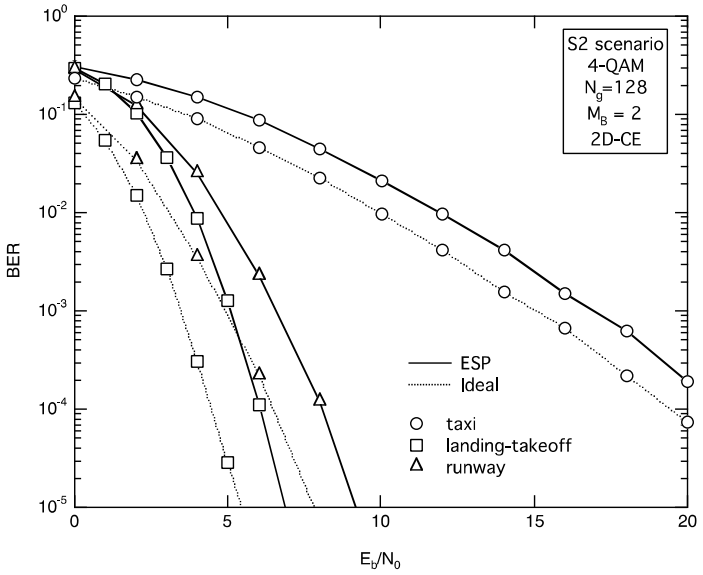

Figure 8: BER for a 4-QAM system endowed with 2D-CE in the FL-S2 scenario.

The results in Figure 9 and Figure 10 are obtained in the same operating conditions of Figure 7 and Figure 8, respectively, except that now the data symbols belong to a 16-QAM constellation. A close inspection of Figure 9 and Figure 10 yields similar conclusions to those of Figure 7 and Figure 8.

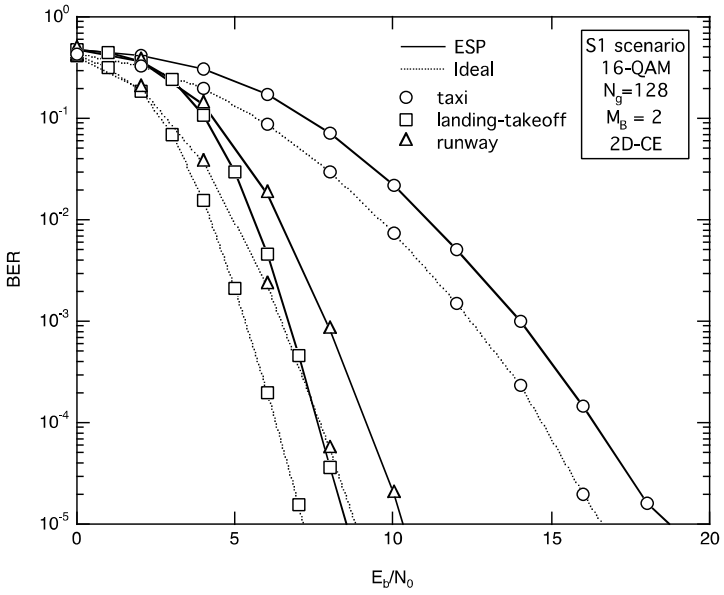

Figure 9: BER for a 16-QAM system endowed with 2D-CE in the FL-S1 scenario.

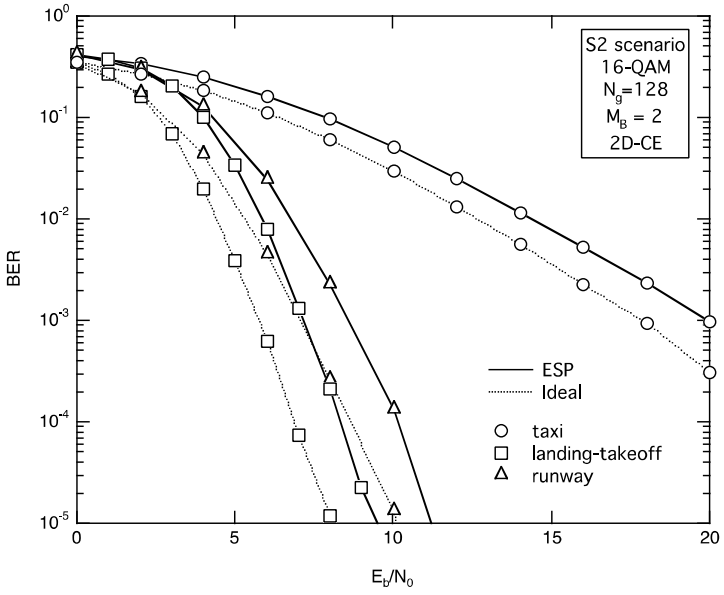

Figure 10: BER for a 16-QAM system endowed with 2D-CE in the FL-S2 scenario.

2.3 Forward Synchronization Analysis

In the sequel, we first recall the synchronization algorithms to be employed in the forward link, and then evaluate their performance over the different propagation channels illustrated in Section 2.1 by means of numerical results.

2.3.1 Detection of the training symbol

The first task that the mobile station (MS) must accomplish during the forward link synchronization phase is the detection of the training symbol within the stream of received samples. As specified in [WiM03], the training symbol is placed at the beginning of each frame (training preamble) and contains *N= 1024* subcarriers with indices *n= 0,1,… N-1*. Out of all available 1024 subcarriers, only a subset of 284 subcarriers is actually modulated by a pseudonoise (PN) BPSK sequence. This sequence is selected among 114 possible choices and univocally identifies the transmitting BS. The modulated subcarriers are separated by a couple of unmodulated (null) subcarriers and there are 86 guard band subcarriers on each side of the signal spectrum. The indices of the modulated subcarriers during the frame preamble are given by

$$i_m = \left|\eta_0 + 3m\right|_N \qquad -142 \le m \le 141 \tag{2.15}$$

where $\eta_0 \in \{0,1,2\}$ is an unknown parameter that designates the preamble carrier-set for identification of the cell sector, while the notation $\left|x\right|_N$ denotes the modulo-*N* operation reducing x to the interval $[0, N-1]$.

The training preamble is preceded by a cyclic prefix (CP) of length N_g = 128. The samples taken taken at the instants $t_k = kT_u / N$ are given by

$$s_p(k) = \frac{A}{\sqrt{N}} \sum_{m=-142}^{141} a_p(m) e^{j2\pi(\eta_0+3m)k/N} \qquad -N_g \le t \le N-1 \tag{2.16}$$

where $\mathbf{a}_p = \{a_p(-142), a_p(-141), ..., a_p(-141)\}$ is the sequence of pilot symbols belonging to the p^{th} preamble (with $p = 0,1,\ldots,113$ and $a_p \in \{\pm 1\}$), while $A = 2\sqrt{2}$ accounts for the power boosting applied to the pilot. We denote by f_Δ the CFO normalized by the subcarrier spacing. The samples received at the MS and corresponding to the training preamble are thus given by

$$r(k) = \frac{A}{\sqrt{N}} e^{j2\pi(f_\Delta+\eta_0)k/N} \sum_{m=-142}^{141} a_p(m) H(i_m) e^{j6\pi mk/N} + w(k) \tag{2.17}$$

with i_m being defined as in (2.15). The quantities $w(k)$ account for thermal noise and are modeled as statistically independent and complex-valued Gaussian random variables with zero-mean and variance σ_w^2, while $H(i_m)$ is the channel frequency response over the i_m^{th} subcarrier.

The detection of the training symbol is performed on the basis of the following metric

$$M(d) = \frac{\left|C(d)\right|}{\max\{P(d), P(d+N_c)\}} \tag{2.18}$$

Where *d* is a time index which slides along in time as the receiver searches for the training preamble while *C(d)* is defined as

$$C(d) = \frac{1}{2N_c} \sum_{k=0}^{2N_c-1} r^*(d+k) r(d+k+N_c) \tag{2.19}$$

and $P(d)$ is obtained as

$$P(d) = \frac{1}{2N_c} \sum_{k=0}^{2N_c-1} \left| r(d+k) \right|^2 . \tag{2.20}$$

In Figure 11 we report numerical measurements illustrating P_{fa} and P_{md} as a function of the threshold λ_0 for the different channel scenarios illustrated in Section 2.1. The SNR is fixed to 0 dB and the CP is composed of 128 samples. As is seen, P_{fa} is virtually independent of the operating scenario and attains the theoretical performance obtained as

$$P_{fa} = \exp(-2\lambda_0^2 N_c). \tag{2.21}$$

Vice versa, P_{md} is largely affected by the scenario under investigation. To ease understanding, we now illustrate how the results illustrated in Figure 11 must be used. Assume for example that a P_{fa}= 10^{-10} is required, which corresponds to λ_0= 0.185 in (2.21)

$$P_{fa} = \exp(-2\lambda_0^2 N_c).$$ (**2.21**). In such a case, it is seen that P_{md} is approximately 10^{-4} for the taxi scenario while it is much smaller than 10^{-4} for both runway and landing-takeoff scenarios. As seen, the best results are obtained for the landing-takeoff channel.

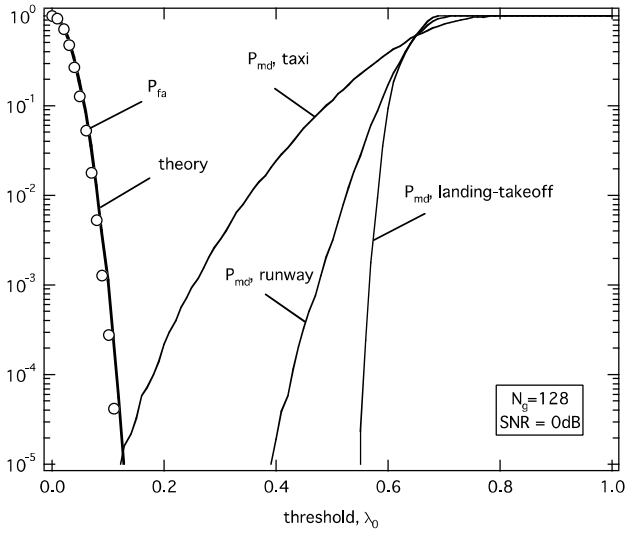

Figure 11: P_{fa} and P_{md} as function of λ_0 with SNR= 0 dB.

2.3.2 Timing Estimation

Assume that the metric *M(d)* overcomes the threshold λ_0 at d= d_0. Then, the receiver starts a timing synchronization procedure whose goal is to identify the beginning of each OFDMA block so as to find the correct position of the DFT window. The timing estimation is performed exploiting the autocorrelation properties that the CP induces on the time domain samples. In practice, the following *N*-lag autocorrelation function is used as a timing metric

$$\gamma(d) = \sum_{k=0}^{N_g-1} r(d+k+N)r^*(d+k) \qquad d_0+1 \le d \le d_0+N_T \tag{2.22}$$

where $N_T = N + N_g$ is the block length (including the CP) expressed in sampling intervals. Since the CP is just a duplication of the last N_g samples of the OFDM block, we expect that $|\gamma(d)|$ exhibits a peak whenever the samples $r(d+k)$ with $0 \le k \le N_g - 1$ belong to the CP. In those applications in which the CP length N_g is relatively small, accurate timing recovery might be difficult to obtain as a consequence of the short integration window employed in (2.22). A possible solution consists of averaging $\gamma(d)$ over a specified number M_B of OFDM block. This produces the following modified metric

$$\overline{\gamma}(d) = \sum_{m=0}^{M_B-1} \gamma(d+mN_T)\,. \tag{2.23}$$

The timing estimate is eventually obtained by looking for the global maximum of $|\overline{\gamma}(d)|$ over a time interval $I = [d_0+1, d_0+N_T]$, i.e.,

$$\hat{d} = \arg\max_{d \in I} \left\{ |\overline{\gamma}(d)| \right\}. \tag{2.24}$$

Numerical results illustrating the probability density function (pdf) of $\hat{d}$ as obtained with N_g= 128 and M_B=*1* for the different operating scenarios are illustrated in, respectively Figure 12. Again, we let SNR= 0 dB. In these experiments, the value *d=0* corresponds to the first sample of the CP and represents the correct timing instant. While, in the landing-takeoff channel the mean of the metric peak is exactly placed at the start of the OFDM symbol (i.e., at *d= 0*), in both taxi and runway channels it is delayed by some samples as a consequence of the channel dispersion. This is confirmed by the fact that $\mathrm{E}\{\hat{d}\} > 0$ in Figure 12 and Figure 14. The numerical results of Figure 14, Figure 15 and Figure 16 are obtained in the same operating conditions of except that now the number of OFDM blocks M_B= 4. As expected, the pdf of $\hat{d}$ becomes narrower as M_B increases due to the improved accuracy of the corresponding timing estimate.

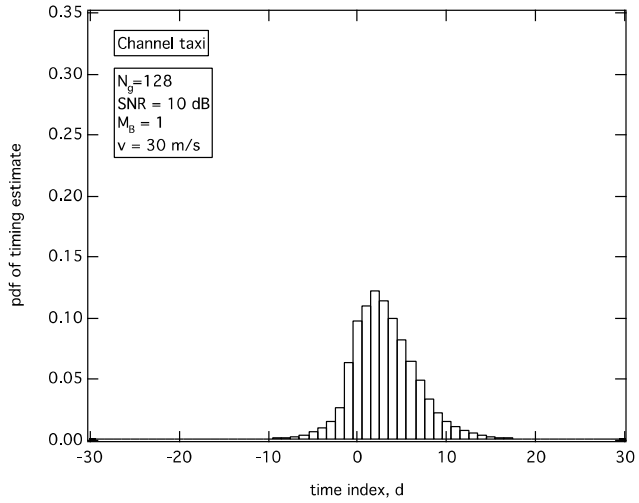

Figure 12: Pdf of the timing estimate with channel taxi, SNR= 10 dB and M_B= 1.

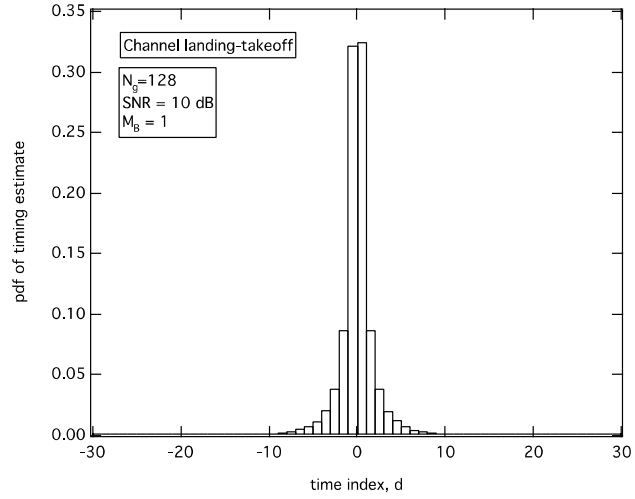

Figure 13: Pdf of the timing estimate with channel landing-takeoff, SNR= 10 dB and M_B= 1.

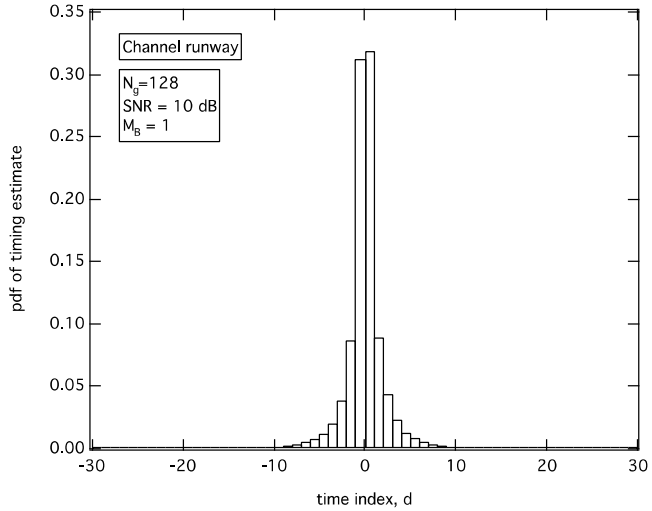

Figure 14: Pdf of the timing estimate with channel runway, SNR= 10 dB and M_B= 1.

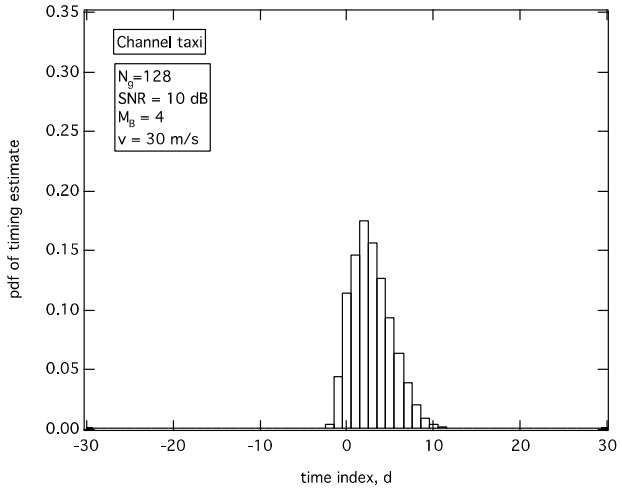

Figure 15: Pdf of the timing estimate with channel taxi, SNR= 10 dB and M_B= 4.

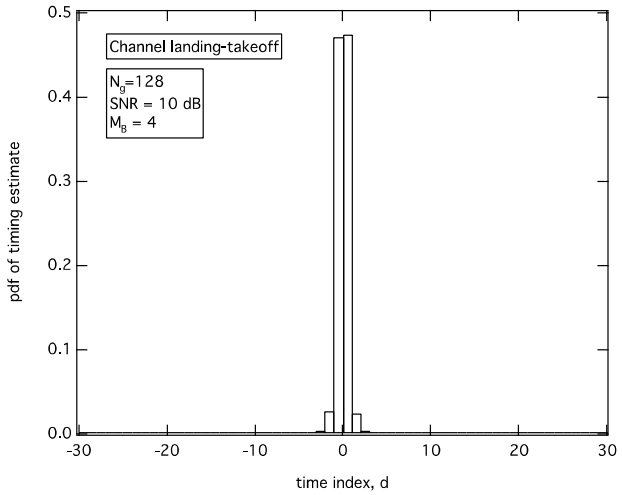

Figure 16: Pdf of the timing estimate with channel landing-takeoff, SNR= 10 dB and M_B= 4.

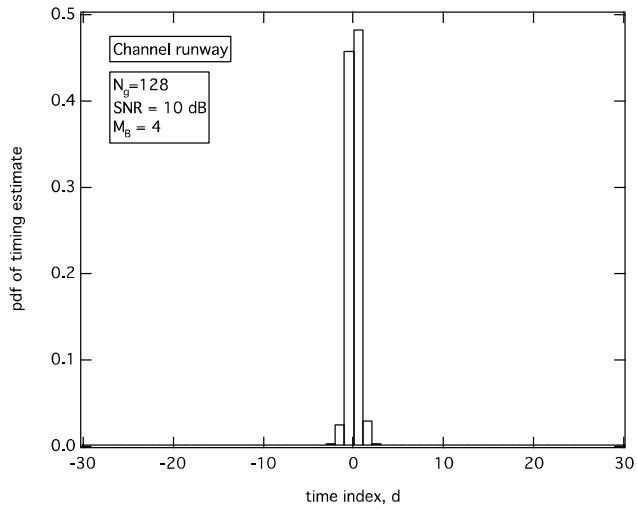

Figure 17: Pdf of the timing estimate with channel runway, SNR= 10 dB and M_B= 4.

We recall that IBI is present during the payload section of the frame whenever the timing estimate $\hat{d}$ lies outside the interval $J_d = [L-1, N_g]$, where L is the channel impulse response length expressed in sampling intervals. Hence, an effective method for reducing the IBI power consists of pre-advancing $\hat{d}$ so as to place the expected value of the timing estimate toward the middle point of J_d, which is given by $(L-1+N_g)/2$. This leads to the following refined timing estimate

$$\hat{d}^{(f)} = \hat{d} - \mathrm{E}\{\hat{d}\} + (L-1+N_g)/2. \tag{2.25}$$

Extensive simulations indicate that $\mathrm{E}\{\hat{d}\}$ is approximately equal to the mean delay associated to the channel response. This parameter is generally unknown at the receiver, but can roughly be approximated by $(L-1)/2$. Using this result into (2.25), yields the final timing estimate in the form

$$\hat{d}^{(f)} = \hat{d} + N_g/2 \tag{2.26}$$

which is eventually employed for a correct positioning of the receive DFT window.

2.3.3 Fractional offset estimation

We begin by decomposing the carrier frequency offset f_Δ into an *integer part* (ICFO), which is multiple of the subcarrier spacing $\Delta f = 1/T_u$, plus a remaining *fractional part* (FCFO), less than $\Delta f/2$ in magnitude. Then, we have

$$f_\Delta = \varepsilon + \mu \tag{2.27}$$

where μ is integer-valued and represents the ICFO, while ε is the FCFO belonging to the interval $(-0.5, +0.5)$. Here, we concentrate on the acquisition of ε, while the problem of estimating the integer offset μ is addressed later.

We begin by considering the timing metric $\overline{\gamma}(\hat{d})$ evaluated at the optimum time instant $\hat{d}$ given in (2.16). Substituting (2.14) into (2.15) and letting $\hat{d}_{k,m} = \hat{d} + k + mN_T$, we obtain

$$\overline{\gamma}(\hat{d}) = \sum_{m=0}^{M_B-1} \sum_{k=0}^{N_g-1} r(\hat{d}_{k,m} + N) r^*(\hat{d}_{k,m}) \tag{2.28}$$

where $r(k)$ are the received samples, which can be expressed as

$$r(k) = s_R(k) e^{j2\pi f_\Delta k/N} + w(k). \tag{2.29}$$

where $s_R(k)$ is the useful signal component. Recalling that $f_\Delta = \varepsilon + \mu$ with μ being integer valued, from **Error! Reference source not found.** we see that an estimate of the FCFO can be computed as

$$\hat{\varepsilon} = \frac{1}{2\pi}\arg\left\{\bar{\gamma}(\hat{d})\right\} \tag{2.30}$$

where $\arg\{X\}$ denotes the *principal value* of the argument.

Figure 18 and Figure 19 illustrate the variance of the frequency estimate $\hat{\varepsilon}$ as a function of the SNR for N_g= 128 and different operating situations. The number of employed OFDM blocks is M_B= 1 in Figure 18 and M_B= 4 in Figure 19. The thick solid line reports the theoretical performance computed as

$$\mathrm{var}\{\hat{\varepsilon}\} = \frac{1}{4\pi^2 M_B N_g}\left(\mathrm{SNR}^{-1} + \frac{1}{2}\mathrm{SNR}^{-2}\right) \tag{2.31}$$

while marks indicate simulation results. We investigate four different operating situations: *i*) transmission over an AWGN channel with perfect timing information (PTI); *ii*) transmission over the taxi channel; *iii*) transmission over the landing-takeoff channel; *iv*) transmission over the runway channel. Results obtained with an AWGN channel model validate the analysis in (2.31) since in this case the samples used to compute $\bar{\gamma}(\hat{d})$ in (2.28) are free from IBI. On the other hand, in the presence of multipath propagation (runway and taxi channel models) the estimation accuracy departs from the theoretical curve and exhibits an irreducible floor due to the insurgence of IBI. Such a floor is not present if the runway channel is considered since in this case the signal is received from a single path. It is worth observing that, in the multipath scenarios, the variance reduces as M_B grows large.

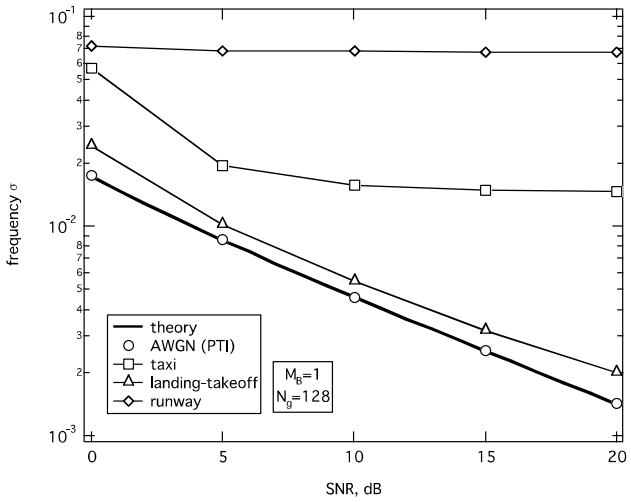

Figure 18: Variance vs. SNR with M_B= 1 and N_g= 128.

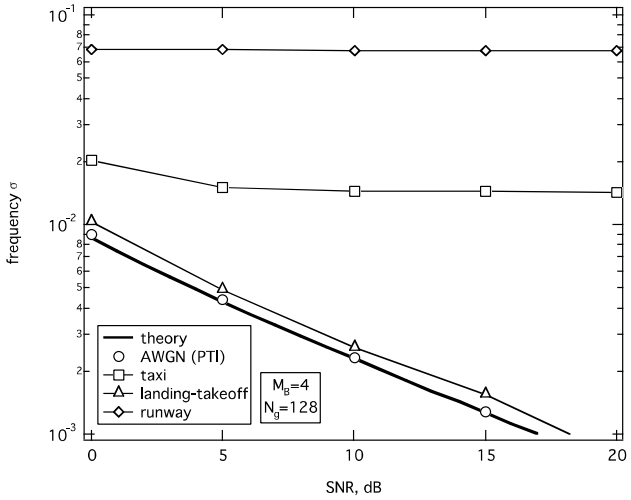

Figure 19: Variance vs. SNR with M_B= 4 and N_g= 128.

2.3.4 Integer frequency recovery and preamble identification

We start using the timing estimate $\hat{d}^{(f)}$ provided in (2.26) in order to select the *N* samples belonging to the received training preamble, say $r(k+\hat{d}^{(f)})$ with *k= 0,1,… N-1*. Next, we counter-rotate the samples $r(k+\hat{d}^{(f)})$ at an angular speed $2\pi\hat{\varepsilon}/N$ so as to compensate for the FCFO. This produces the frequency-corrected samples

$$x(k)=r(k+\hat{d}^{(f)})e^{-j2\pi k\hat{\varepsilon}/N} \qquad k=0,1,\ldots,N-1 \tag{2.32}$$

which are then fed to the DFT unit, yielding the frequency-domain samples

$$X(n)=\frac{1}{\sqrt{N}}\sum_{k=0}^{N-1}x(k)e^{-j2\pi nk/N} \qquad n=0,1,\ldots,N-1. \tag{2.33}$$

To proceed further, we consider the situation where the p^{th} training preamble $\{a_p(m);-142\le m\le 141\}$ is transmitted (with *p*= 0,1,… 113) and define the following zero-padded sequence

$$a_p^{(ZP)}(n)=\begin{cases}a_p(m) & \text{if } n=i_m\\ 0 & \text{otherwise}\end{cases} \tag{2.34}$$

with $i_m=\left|\eta_0+3m\right|_N$ for $-142\le m\le 141$. Then, assuming ideal FCFO compensation and recalling that the ICFO results into a shift of the subcarrier indices at the DFT output, we may write

$$X(n)=AH(n+\mu)b_p(n+\mu)e^{-j2\pi\delta_d(n+\mu)/N}+W(n) \tag{2.35}$$

where $A=2\sqrt{2}$ is the power boosting factor and $b_p(n)$ is the periodic repetition of $a_p^{(ZP)}(n)$ with period *N*. Also, $W(n)$ is the contribution of the thermal noise while δ_d is the timing error, which appears as a

linear phase shift across the subcarriers. As anticipated, we aim at jointly estimating the ICFO $\mu \in J_\mu$ and the training index $p \in J_p = \{0,1,\ldots,113\}$. One possible approach consists of looking for the global maximum of the objective function

$$\Phi(\tilde{\mu},\tilde{p}) = \left| \sum_{n=3}^{N-1} Y_{\tilde{p}}(n;\tilde{\mu}) Y_{\tilde{p}}^{*}(n-3;\tilde{\mu}) \right|^2 \tag{2.36}$$

with respect to $(\tilde{\mu},\tilde{p}) \in J_\mu \times J_p$, where $Y_{\tilde{p}}(n;\tilde{\mu})$ is the product of the DFT output with the hypothesized shifted sequence $b_{\tilde{p}}(n+\tilde{\mu})$, i.e,

$$Y_{\tilde{p}}(n;\tilde{\mu}) = X(n) b_{\tilde{p}}(n+\tilde{\mu}). \tag{2.37}$$

The estimated values of μ and p are thus given by

$$(\hat{\mu},\hat{p}) = \arg \max_{(\tilde{\mu},\tilde{p}) \in J_\mu \times J_p} \{\Phi(\tilde{\mu},\tilde{p})\}. \tag{2.38}$$

In order to assess the performance of the estimator (2.38), we consider the probability that $(\hat{\mu},\hat{p})$ does not coincide with the true values (μ,p), say $P_e = \Pr\{(\hat{\mu},\hat{p}) \neq (\mu,p)\}$. Figure 20 and Figure 21 illustrate P_e as a function of the SNR for the different investigated scenarios with M_B= 1 and M_B= 4, respectively.

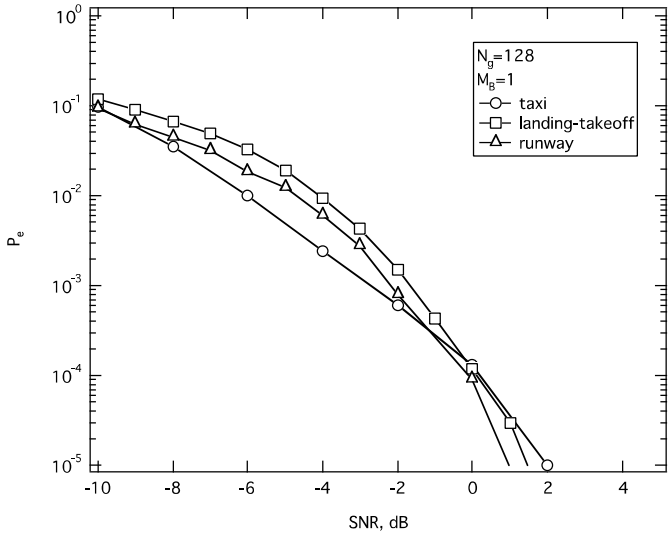

Figure 20: Probability of an estimation failure vs. SNR with M_B= 1 and N_g= 128.

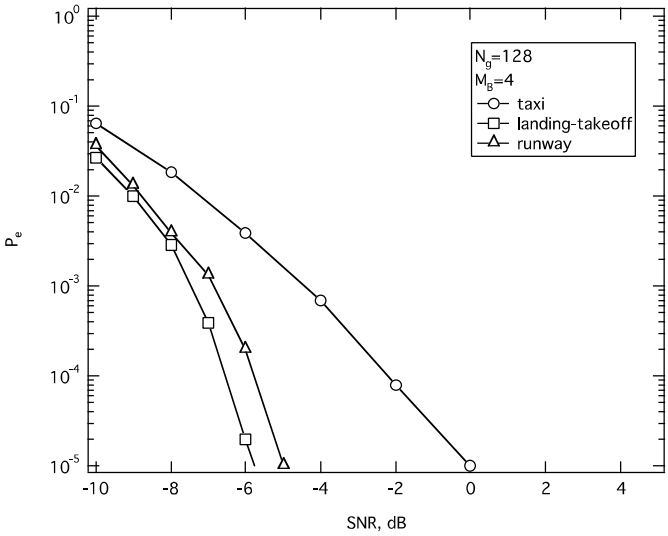

Figure 21: Probability of an estimation failure vs. SNR with M_B= 4 and N_g= 128.

2.4 Summary

In this section, we have investigated the performance of AeroMACS during the take-off, landing, and approach phases, assessing the potential exploitation of the system at these stages. We tailored the investigations to the forward link case, as AeroMACS can be used for transmission only by aircraft being on the ground. The main peculiarities of these scenarios have been evaluated, and new channel parameters for the SANDRA channel model developed during the first phase of the WP have been extrapolated for the simulation analysis. We focused first on the general performance of the system and then on the synchronization analysis.

The general performance of the system has been evaluated in term of BER vs. E_b/N_0 for both the new channel scenarios. Numerical results obtained by computer simulations show good performance of the system in the new environment. Generally, the results obtained with the adopted channel estimation algorithm (2D-CE) present a loss of almost 2 dB with respect to the ideal case of perfect channel knowledge[6]. The curves representing the runway and landing scenarios outperform the one characterizing the taxi case. This behaviour may be explained considering the higher Rice factor values, and the increment of diversity introduced by the higher speeds.

Finally, the investigation has been addressed to the analysis of the synchronization that constitutes a challenging operation in high speed conditions. The performance of the synchronization algorithms have been assessed in the new scenarios, illustrating probability of false alarm, probability of misdetection, timing offset, frequency offset, and probability of failure. Additionally, the numerical results obtained by

[6] This result is obtained for all the channel scenarios.

computer simulations are compared with the results obtained for the taxi scenario. The probability of false alarm obtained with the proposed algorithm provides ideal performance for all the scenarios. The probability of misdetection depends on the scenario; however, the take-off/landing airborne scenario provides the best results. The probabilities of an estimation failure obtained for the different scenarios are similar when M_B=1 is used. Increasing M_B to 4, the results improve, however, the runway and take-off/landing cases are subjected to a greater improve (indeed, for M_B= 1, all the cases show P_e= 10^{-4} at SNR= 0 dB, for MB= 4, P_e= 10^{-4} is obtained at SNR= -3.5 dB by the taxi case, SNR= -6.5 dB by the runway case, and SNR= -7.5 dB by the take-off/landing case). The numerical results illustrate good estimation accuracy in every considered scenario.

3 Exploitation of AeroMACS Base Stations for Target Identification and Positioning

In this section, passive radar functionality making use of AeroWiMACS signals as sources of opportunity will be investigated. Radar ambiguity function will be defined to estimate the spatial resolution as well as artefacts due to synchronization pilot tones. Radar coverage of a single system will be computed in term of SNR and spatial resolution.

3.1 Passive Radar system

Passive radar system, also referred to as passive coherent location system (PCL) exploits reflections from illuminators of opportunity in order to detect and track objects. Among all the potential signals of opportunity, we can mention FM radio, DAB/DVB-T, GSM, Wi-Fi, communication or navigation satellites. A PCL receiver, as shown in Figure 22, generally presents two receiving channels denoted as the reference and target channels. The reference channel is used to capture the direct signal from the transmitter and provides a reference signal to be compared with the target return.

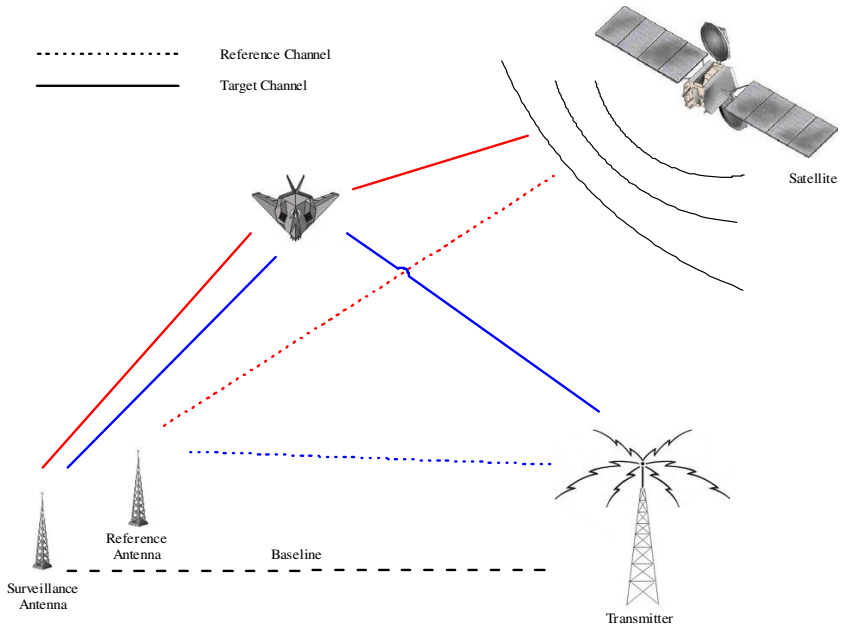

Figure 22: Passive radar scenario

The comparison is usually carried out by a cross-correlation between the reference signal and the target signal and it actually represents the basic process to detect targets with passive radar. Some of the most interesting applications of these systems include: atmospherics studies, maritime and air surveillance, oceanography, monitoring of public areas such as railways and airport terminal. The application area of passive radars is strictly dependent on the illuminator of opportunity properties. The important features of an illuminator of opportunity are: the power density values at the target, the coverage, the signal characteristics, and its ambiguity properties. By analyzing the transmitted power of the illuminator of opportunity, it is possible to determine the surveillance area that PCL can cover. The most effective mathematical tool used for studying the radar performances of a given waveform is the ambiguity function. By means of the ambiguity function, range and Doppler resolutions are directly obtained.

3.2 AeroMACS Signal Generation

The IEEE 802.16 Wireless MAN standard [WiM03] provides specifications for an air interface for fixed, portable and mobile broadband wireless access systems. WiMAX transmissions include OFDMA technology. Unlike many other OFDM-based systems such as WLAN, the standard supports variable bandwidth sizes. The standard supports multiple schemes for allocating the resources to the users. Each frame is divided in down link (DL)[7] and uplink sub-frames, separated by transition gaps. The sub-frames are divided in sub-channels, according to different subcarriers allocation modes. The partially use of subcarriers (PUSC) mode,

[7] In the aeronautical context, the nomenclature down link (DL) and forward link (FL) is not used in order to avoid misunderstanding. In this context, we refer to the link from the base station to the mobile station (called in conventional mobile system DL) as forward link. The returning link from the mobile station to the base station is called reverse link (RL).

defined for the DL (i.e. FL), uses a cluster structure to assign the pilots position, as illustrated in Figure 6. A WiMAX forward link PUSC signal has been simulated with a Simulink model, as illustrated in Figure 23. The simulation parameters are reported in Table 4.

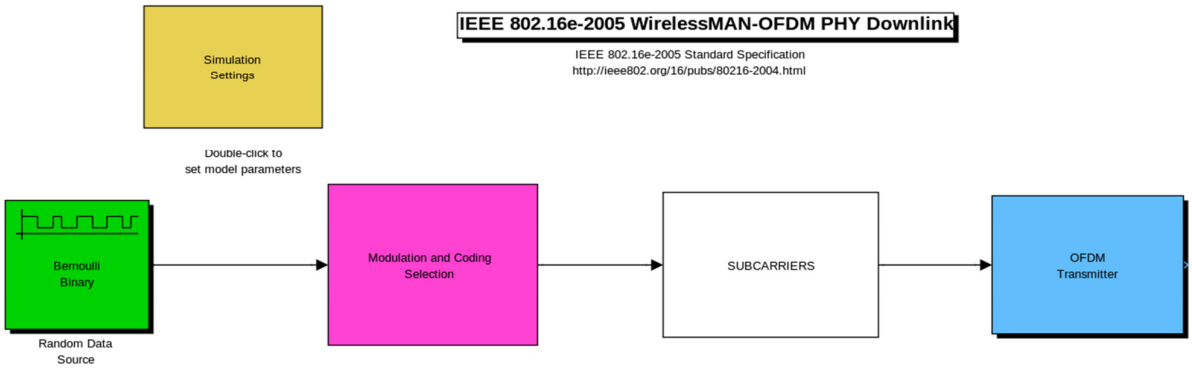

Figure 23: AeroMACS simulator

Table 4: AeroMACS simulation parameters

Simulation Parameters	Values
System Bandwidth/ FFT Size (NFFT)	10 MHz/ 1024
Sampling Frequency	11.2 MHz
Subcarrier Spacing (Δf)	10.94 KHz
Useful symbol Time (T_b)	91.4 µs
Guard Time ($T_g=T_b/8$)	11.4 µs
Symbol Time ($T_s=T_b+T_g$)	102.8 µs

The spectrum of the signal is pass-band, with a nearly rectangular envelop, as shown in Figure 24.

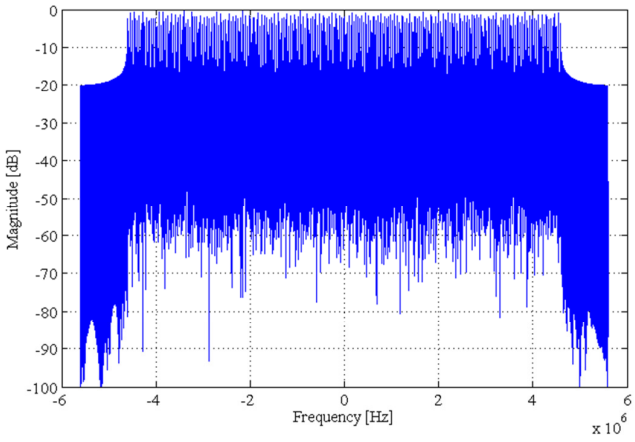

Figure 24: AeroMACS spectrum

3.3 Ambiguity Function Analysis

Resolution and ambiguity in both range and Doppler are parameters of fundamental importance in the design and performance achievement of any radar system. In passive coherent location (PCL) systems, these properties are determined by the transmitted waveform, the location of the transmitter, the location of the receiver and the location of the target. The ambiguity function represents the output of a matched filter and may be written as:

$$\chi_{rd}(\tau, f_d) = \left| \int_0^{T_{\text{int}}} s_r(t) s_d^*(t+\tau) e^{j2\pi f_d t} dt \right|^2 \tag{3.1}$$

where $\chi_{rd}(\tau, f_d)$ is the ambiguity response at delay τ, Doppler f_d and $s_r(t)$ is the received signal and $s_d(t)$ is the direct (or reference) signal. In practice the ambiguity function is often digitally implemented on a computer and the equation becomes:

$$\chi_{rd}(\tau, f_d) = \left| \sum_{n=0}^{N-1} s_r[n] s_d^*[n+\tau] e^{j2\pi f_d n T_s} \right|^2 \tag{3.2}$$

where $s_r[n] = s_r[nT_s]$, $s_d[n] = s_d[nT_s]$, T_s is the sample period and N in the number of samples in the integration time $(T_{\text{int}} = T_s N)$. A simulated ambiguity function is shown in Figure 25.

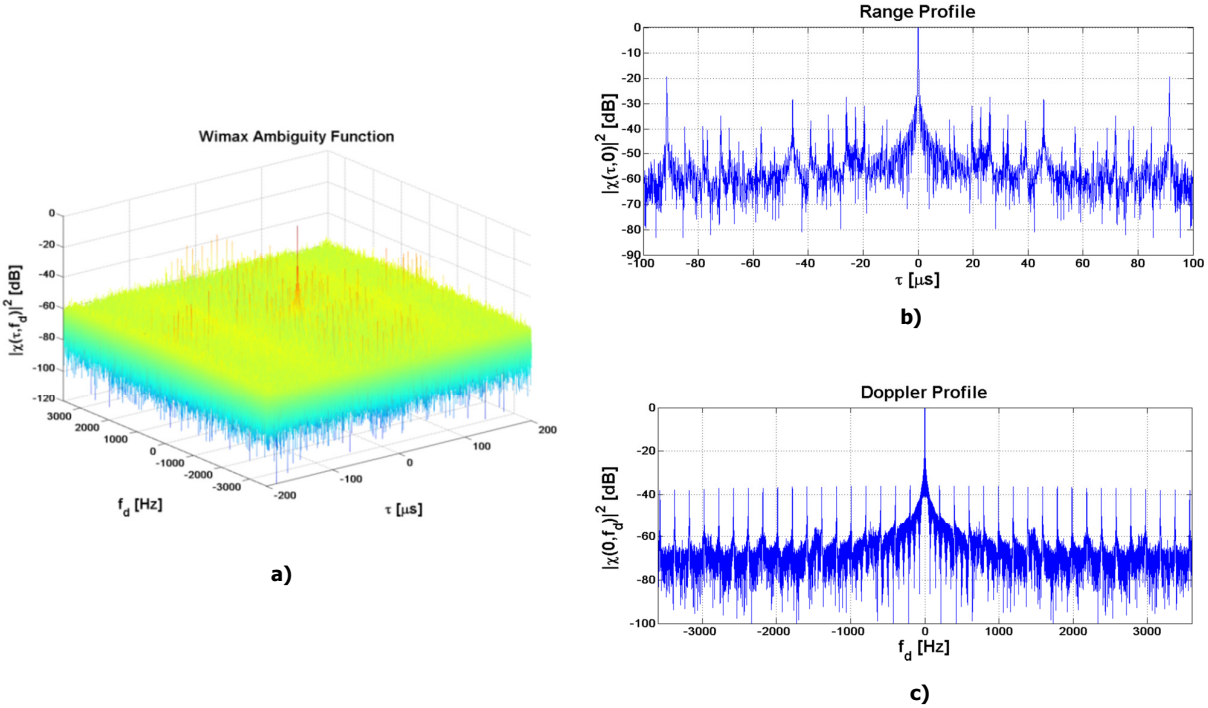

Figure 25: AeroMACS signal ambiguity function. a) 3D view, b) Range profile, c) Doppler profile.

The specific structure of the AeroWiMACS signal, and specifically the presence of guard intervals and pilot tones, introduces a number of undesired deterministic peaks in the Ambiguity Function (AF) as shown in Figure 25, which might yield significant masking effects on the useful signal and produce false alarms.

The simulations have proven that the theoretical range resolution is around 15 m or 0.1 µs as shown in Figure 26. While the Doppler resolution depends on the integration time and in this case with $T_{\text{int}} = 0.5s$ is equal to 2 Hz (Figure 27).

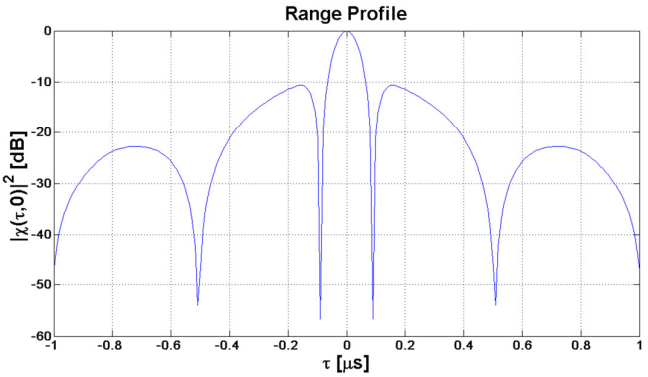

Figure 26: Ambiguity function range profile zoom view

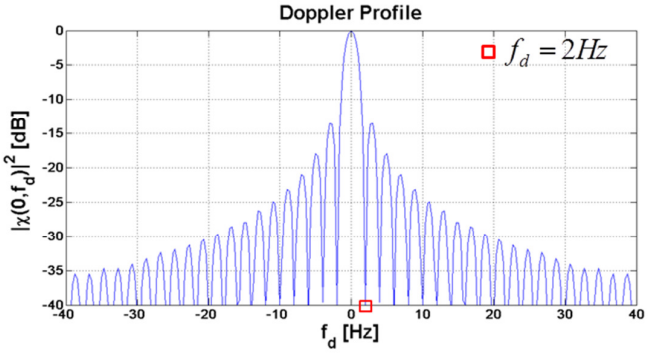

Figure 27: Ambiguity function Doppler profile zoom view.

3.4 Implementation of Deterministic Peaks Removal Technique

Target detection in a PCL system is mainly based on the evaluation of the two-dimensional cross-correlation function between the surveillance signal and the reference signal. Thus, according to the analysis presented in the previous section, the detection performance of AeroMACS based passive radar may be strongly limited by the strong side-peaks appearing in signal AF which might be responsible for significant masking effects even in the presence of large range-Doppler separation.

The technique proposed here exploits a filtering based on the estimation of the power spectral density (PSD) of a typical AeroMACS signal, and the PSD of signal composed only by random components (RC), without pilots and guard interval. Figure 28 shows the pre-processing algorithm block diagram.

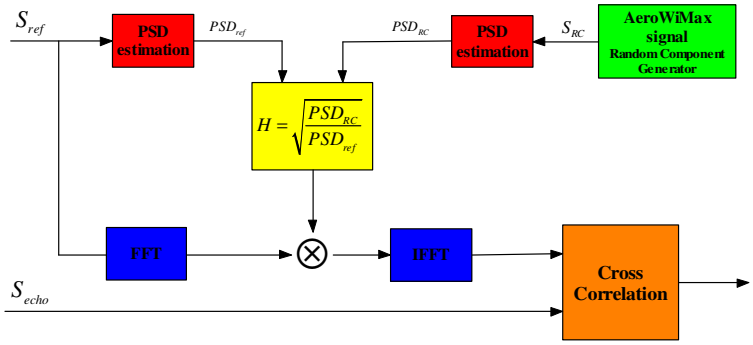

Figure 28: Simplified pre-processing block diagram

Figure 29b shows the range profile of the AF after pre-processing and in this case the range ambiguities have been strongly attenuated. Defining the ambiguity function parameter side peaks reduction (SPR) as:

$$SPR = \frac{\sum_{i=1}^{N_{sp}} |\chi_{NF}(\tau_i, 0)|_{dB}}{\sum_{i=1}^{N_{sp}} |\chi_F(\tau_i, 0)|_{dB}} \tag{3.3}$$

where χ_{NF} is the Not Filtered ambiguity function, χ_F is the filtered ambiguity function, N_{SP} is the number of side peaks of the ambiguity function and τ_i is the delay relative to the i-th side peak. For the here proposed pre-processing technique, the SPR value is about 30 dB.

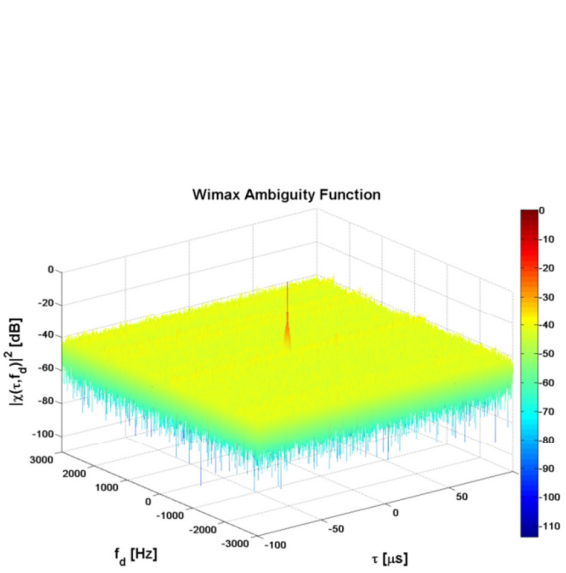

a)

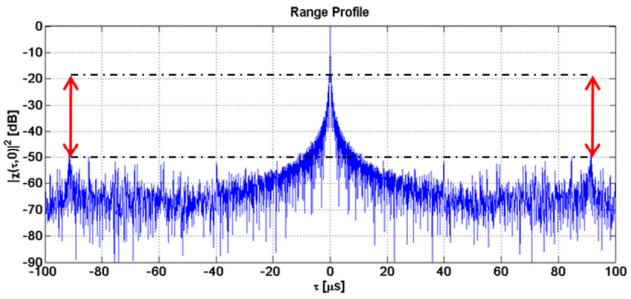

b)

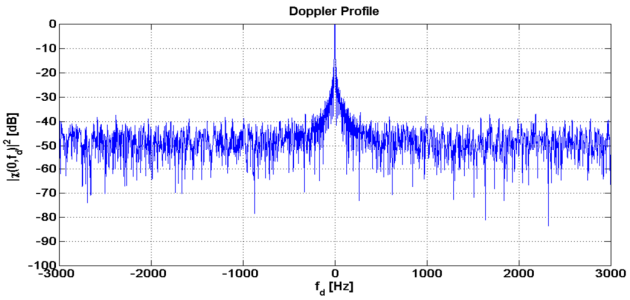

c)

Figure 29: AeroMACS ambiguity function after pre-processing. a) 3D View, b) Range profile, c) Doppler profile

The proposed technique improves the range profile of AF and maintains the same performance in the Doppler domain (Figure 29b).

3.5 Coverage Analysis

Considering a bistatic configuration, the SNR in the integration time T_{int} can be evaluated by means of:

$$SNR = \frac{ERP\ G_r \lambda^2 \sigma_b}{(4\pi)^3 r_1^2 r_2^2 k T_0 F_n L} T_{\text{int}} \tag{3.4}$$

where $ERP = P_t G_t$ is the effective radiated power, P_t is the transmitted power, G_t is the transmission gain $G_r = 20dB$ is the receiver gain $\sigma_b = 1m^2$ is the bistatic radar cross section, $\lambda = 0.0588m$ is the carrier wavelength, r_1 is the transmitter to target distance, r_2 is the target receiver distance, $F_n = 5dB$ is the noise figure, $L = 5dB$ are system losses $T_0 = 290°K$, k is the Boltzmann constant. The baseline length (transmitter-receiver distance) is about 200m.

Figure 30 shows the obtained SNR for different values of transmitted power and effective isotropic radiated power. In particular, EIRP values equal to -25 dB, -10dB, 5dB, and 15dB are considered.

A SNR of 18 dB has been considered to guarantee a probability of detection $P_D = 80\%$, and a probability of false alarm $P_{FA} = 10^{-6}$ for Swerling I target model. By varying the transmitted power, the coverage of the passive radar AeroMACS based spans between 700 m and 5 km, as illustrated in Figure 30. The thumbtack shape of the AeroMACS ambiguity function guarantees a good range resolution of about 15 m. Therefore, the AeroMACS signal could represent a good candidate for short range passive radar applications.

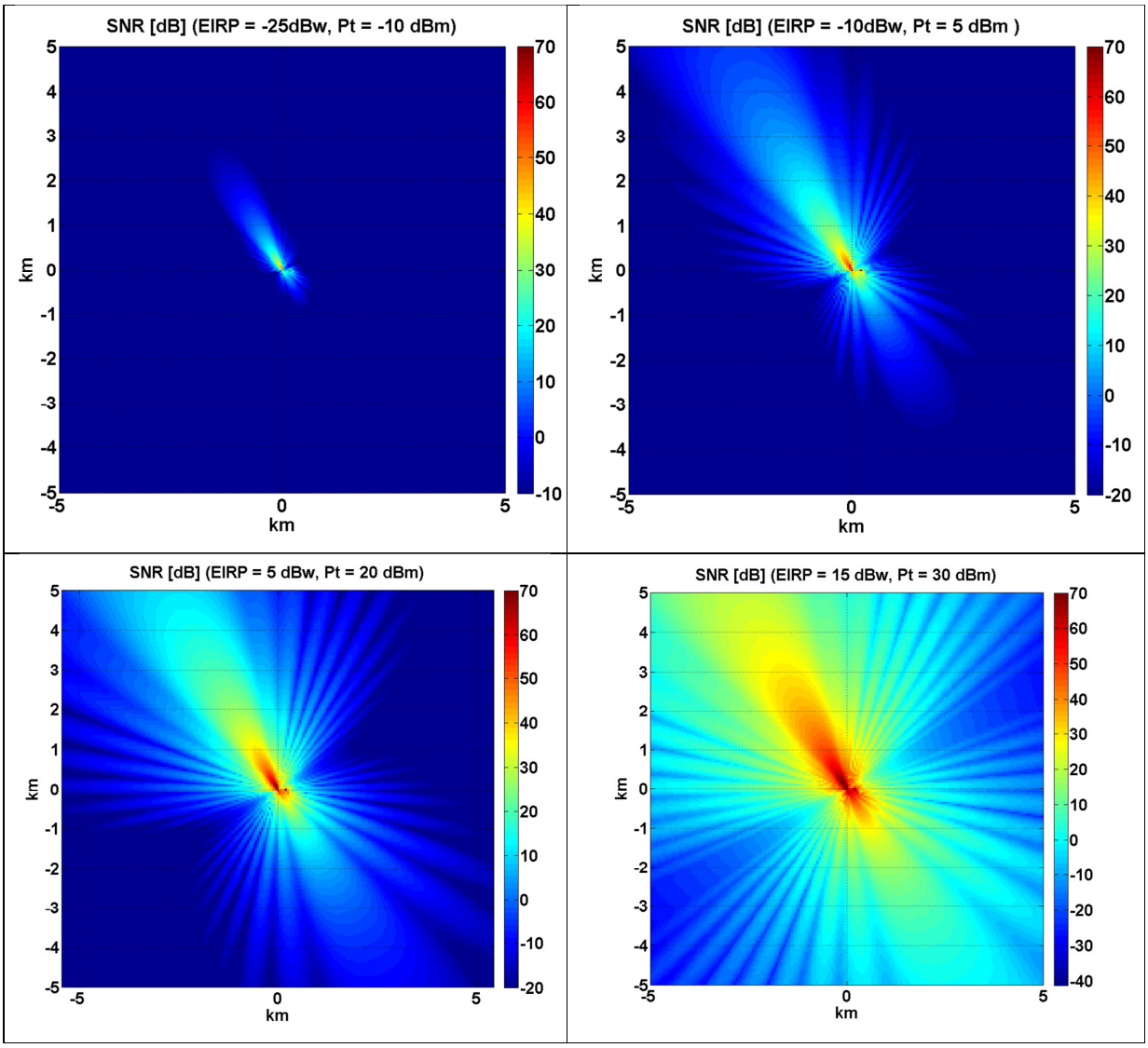

Figure 30: Expected SNR Maps for different EIRP/P_t values.

4 Investigation on Potential AeroMACS Enhancements

In this chapter, we targeted the long term AeroMACS evolution by analysing potential methods for enhancing the performance of the system. Improvements of the system could be advantageous in the optic of future stronger demands as higher quality of service or capacity.

In this analysis, we focused on solutions that increase the performance of the system by exploiting diversity techniques. In the deliverable SANDRA_D6.2.1 [D6.2.1], we extendedly analyzed the performance of AeroMACS, and we observed that the most critical results correspond to the channel scenario having less diversity. Following these outcome, we tackled this problem investigating potential solutions for increasing the diversity of the system, and therefore improving the performance of the system.

We accounted different forms of diversity as time diversity and space diversity. Since the use of multiple antennas on the aircraft is seen to be critical[8], we investigated an alternative solution that achieves spatial diversity by means of cooperative communications.

The next subsections illustrate in detail the analysis on the application of packet-level coding and cooperative communications techniques to AeroMACS.

4.1 Packet-Level Coding

In many applications, erasure correcting codes are used to recover packet losses at high protocol stack layers. The objects (e.g. files) to be transmitted often have variable sizes, resulting in a variable number of packets to be encoded by the packet-level encoder. In this chapter, algorithms for the (on-line) flexible design of parity-check matrices for irregular-repeat-accumulate codes are investigated. The proposed algorithms allow designing in fast manner parity-check matrices that are suitable for low-complexity maximum-likelihood decoding. The code ensembles generated by the proposed algorithms are analyzed via extrinsic information transfer charts. Numerical results show how the designed codes can attain codeword error rates as low as 10^{-5} without appreciable losses w.r.t. the performance of idealized maximum-distance separable codes. The proposed packet level coding (PLC) approach is applied to the FL of AeroMACS, showing large performance improvement and proving the efficiency and the flexibility of the method. The FL represents in fact an ideal application case for the proposed packet erasure recovery scheme, due to the demand of high reliability, the airport channel characteristics (dominated by harsh fading and frequent shadowing conditions), the large population of aircraft terminals and the multicast nature of part of the traffic (which renders packet-level coding an appealing alternative to retransmission protocols [BYE02, MET84]). As a further remarkable added value, the proposed approach can be applied on top of the existing standard protocol stack, thus it does not require any expensive modification of the off-the-shelf hardware[9].1

4.1.1 Fundamentals of Packet Level Coding Techniques

The application of error control codes to protocol stack layers different from the physical one gained a large interest during the past decade [LUB97, BYE02, LUB06, SHO06, LIV10]. Such coding techniques deal with the use of a linear (block) code applied to encoding units (symbols) that are usually packets with constant size. In this context, a packet level encoder receives as input a set of k packets, and produces as output n>k packets. Figure 31 illustrates and summarize the main packet-level coding principles. Assuming systematic encoding, the final set of packets comprises the k information packets together with m= n – k

[8] The use of multiple antennas and in particular simple schemes that foresee multiple antennas only on the control tower has also been accounted in the previous AeroMACS analysis illustrated in SANDRA_D.2.2.1 [D621].

[9] A software implementation of maximum likelihood (ML) decoders for LDPC codes over packet erasure channels attaining data rates of 1.5 Gbps or more has been demonstrated in [MAT09].

parity packets. At the receiver, after the physical layer decoding, the packets that have been validated (e.g. by an error detection code) are forwarded to the packet level decoder. The corrupted packets are discarded. Therefore, the upper layers deal with packet erasures. The packet level decoder may recover the erased packets by means of the parity packets.

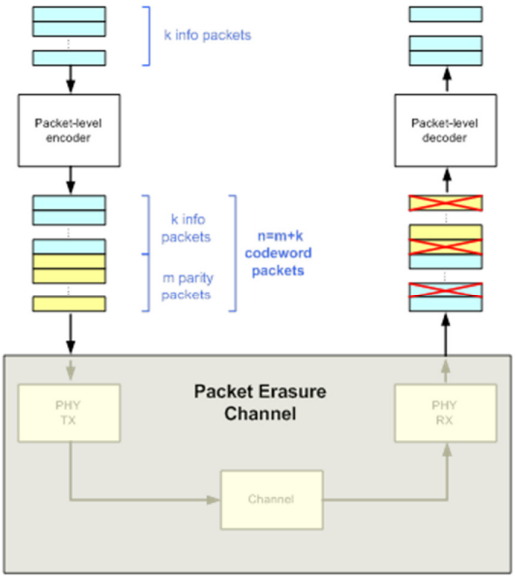

Figure 31: Packet-level coding scheme

Packet-level coding principles

1. The message (e.g., video stream, file) is divided in packets
2. The packet-level encoder encodes k info packets generating m parity packets
3. The packets (info&parity) are protected by physical layer codes and sent over the channel
4. At the receiver, physical layer error correction takes place. Unrecoverable packets are marked as lost (e.g. CRC check)
5. The packet level decoder operates on a virtual erasure channel.
6. If a sufficient amount of packets is received, the packet-level decoder recovers the original message

Packet level codes are employed in multimedia wireless broadcasting systems as the DVB-H/SH standards [FAR06, DVB07], in multicast scenarios [3GPP05], and are also currently investigated in space communication systems [CAL07, DEC07, DEC11].

4.1.2 Application of Packet-Level Coding to AeroMACS

We investigated the use of packet-level coding techniques within the airport communications. This environment, in fact, includes a large population of aircraft terminals, and a traffic composed by unicast, multicast, and broadcast transmissions. Packet-level coding techniques might hence be particularly useful whenever large amounts of information have to be broadcasted to several aircrafts, efficiently complementing Automatic Repeat reQuest (ARQ) protocols [BYE02, MET84]. In this case, the excellent performance of flexible irregular repeat accumulate (F-IRA) rate-compatible families represents a valuable alternative to Fountain coding schemes [BYE02].

We analyzed the performance of packet-level coding techniques in the airport environment by applying the method proposed in [LIV11a] [LIV11b] to the AeroMACS system. The used method presents the further advantage of being flexible, and therefore adaptable to whatever size of the source packets [COCR].

A class of powerful erasure correcting codes is represented by low-density parity-check (LDPC) codes [GAL63]. In fact, it has been demonstrated that some LDPC code ensembles can asymptotically approach with an arbitrarily small gap the binary erasure channel (BEC) capacity under iterative (IT) decoding. Some problems, however, arise when constructing finite length (n, k) LDPC codes according to asymptotically optimal ensembles. Due to the sub-optimality of the IT decoder, at high error rates the performance curve, though usually good, denotes a coding gain loss with respect to that of the same code under maximum likelihood (ML) decoding. In [LIV11a, LIV11b], new techniques were introduced, aiming a fast, on-the-fly, algorithmic construction of the LDPC code parity-check matrix with the largest possible flexibility in the choice of the codes dimension and block length. In fact, in many applications the object (e.g., the file) to be transmitted has a variable size, resulting in a variable number of packets to be encoded. One may design a code with large input block size k and may perform code shortening for all the cases where the number of packets to be encoded is lower. In a similar manner, if the code rate has to be adapted to specific channel conditions, a low-rate code may be designed, and higher rates may be obtained by puncturing. However, shortening does not allow complete flexibility, since a maximum value of k has to be a-priori selected. Moreover, the selection of the codeword symbols to be zero-padded has to be performed in a careful manned to avoid degradations of the IT decoding threshold[10]. Thus, a flexible on-line code construction technique which allows designing in a fast (algorithmic) manner reasonably-good parity-check matrices for an arbitrary set of the (n, k) parameters[11] represents an appealing solutions for different applications.

The code construction is based on a simple algorithm available at both the receiver and the transmitter and the adaptive packet level coding scheme may work as follows. Once the encoder receives the set of k packets to be encoded and the target code rate R= k/n is selected, the set of parameters {n, k, κ} is signaled to the receiver, being κ a parameter that drives the code construction. On the transmitter side, a code $\mathscr{C}$(n, k, κ) is generated and used to encode the set of k packets. At the receiver, the {n, k, κ} parameters are used to reconstruct the parity-check matrix of $\mathscr{C}$(n, k, κ), which is then used for the erasure decoding. The parameters {n, k, κ} can be signaled, for instance, in the packets header. The code construction leads to IRA codes [JIN00] whose parity-check matrix is built according to specific (code-rate dependent) degree distributions. The proposed codes are called flexible IRA (F-IRA) codes. The

[10] Recall that a large gap between the IT decoding threshold and the binary erasure channel (BEC) Shannon limit is responsible on one hand of poor performance under IT decoding, and on the other hand of a large decoding complexity when ML decoding is used [PAO08].

[11] A similar approach has been adopted for the Raptor codes standardized in the multimedia broadcast multicast service (MBMS) [SHO06, 3GPP05] standard.

construction of the F-IRA codes parity-check matrix is based on a pseudo-random approach. With this respect, the parameter κ can be regarded as the seed for the pseudo-random number generator used for the construction of the code parity-check matrix. The proposed approach allows tightly approaching the Singleton bound on the memory-less binary erasure channel (BEC). The complete description of the adopted algorithms can be found in [LIV11a] [LIV11b].

For our investigation, we focused first on the most challenging airport scenario (i.e. the parking one [PUL10a]), which is characterized by non-line-of-sight conditions and slow fading. Here, packet-level coding can enhance the system performance, allowing coding on large blocks and thus exploiting time diversity. Note that an alternative approach for counteracting slow fading is provided by (long) physical layer interleavers (as for instance in the DVB-SH standard, [DVB07]. However, being packet level coding applied on high protocol stack layers, it avoids any problematic modifications of the AeroMACS radio interface. For our simulations, we considered the physical layer of the AeroMACS system baseline, composed by OFDMA symbols of 512 subcarriers with a bandwidth of 5 MHz. We adopted forward link sub-frames of 24 OFDMA symbols, cycle prefix (CP) of 1/8 of the symbol length, and QPSK sub-carrier modulation. Convolutional coding with rate 1/2 is applied to the user packets, which are assumed equal to 10 sub-channels (corresponding to 960 bits). The channel estimation is a linear pilot interpolation in the frequency domain, tailored to the WiMAX frame structure. The performance of the system (without packet-level coding) is depicted in Figure 32, in terms of packet error rate (PER) vs. E_b/N_0. The limited time diversity leads to a lack of steepness in the curve. A PER$\simeq 10^{-2}$ is achieved at E_b/N_0= 12 dB. Note that according to simulation parameters, since the overall frame of 48 OFDMA symbols is 5 ms, the duration of a FL sub-frame is 2.5 ms, while the channel coherence time is roughly 50 ms. We hence applied different packet-level codes directly at the link layer (i.e., considering as encoding symbols the units encoded by the convolutional code). We selected code rates between 4/5 and 19/20, and block sizes of 250, 500 and 1000 symbols (i.e. packets). Considering a frame duration of 5 ms (which includes both the FL and the RL sub-frames), the latency introduced by the packet-level codes spans from 1.25 s (for n= 250 symbols) to 5 s (for n= 1000 symbols), bringing sufficient time diversity to counteract moderate-short outages. The introduced latency is indeed acceptable for file delivery applications, while it is too large for delay-sensitive applications (such as voice communications). The Singleton bound[12] is also provided as reference. The PBC codes attain in almost all the cases the Singleton bound. Figure 32 illustrates the PER vs. E_b/N_0 for different rate-9/10 PBC IRA codes of different lengths. Again, the performance achievable with idealized MDS codes (Singleton bound) is provided as reference. Already with a block length of 250 symbols, the PBC allows tightly approaching the bound. The gain at PER$\simeq 10^{-2}$ w.r.t. the curve without packet-level coding is $\sim$ 2.5 dB.

[12] The Singleton bound represents the performance of an idealized MDS code with a given block length, n, and code dimension k. More specifically, for each set of (n, k) parameters, we analyzed the sequence of packet erasures after physical layer decoding, and we assumed that in a block of n packets, is n−k or less have been erased, the entire block is recovered.

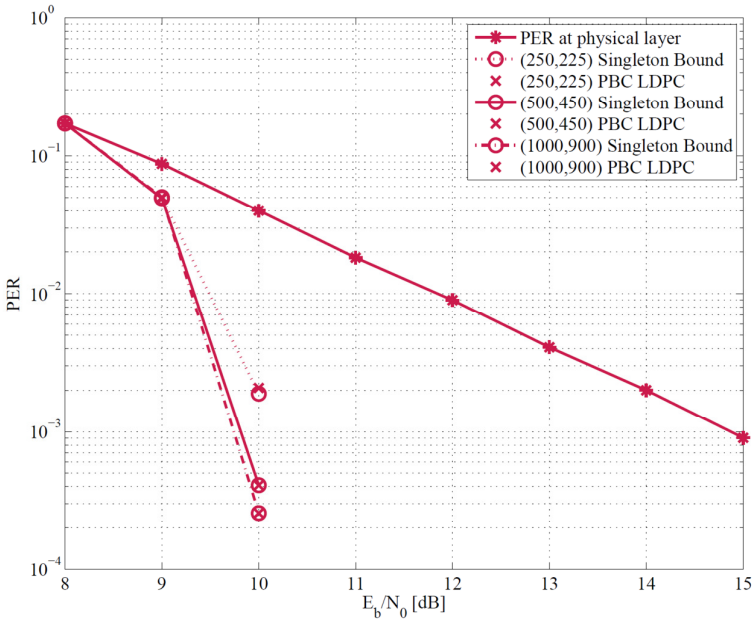

Figure 32: Packet error rate after physical layer decoding, and after the application of the proposed 9/10 packet-level IRA codes (various block lengths).

Moreover, we simulated the performance of AeroMACS with the F-IRA code construction in the NLOS channel scenario developed in [D622]. The performance obtained with the proposed PLC approach in the NLOS scenario is shown in Figure 33. We showed the results obtained with different block coding rates, in particular R=0.9 (n=500, k=450), R=0.9 (n=1000, k=900), and R=0.8 (n=1000, k=800).

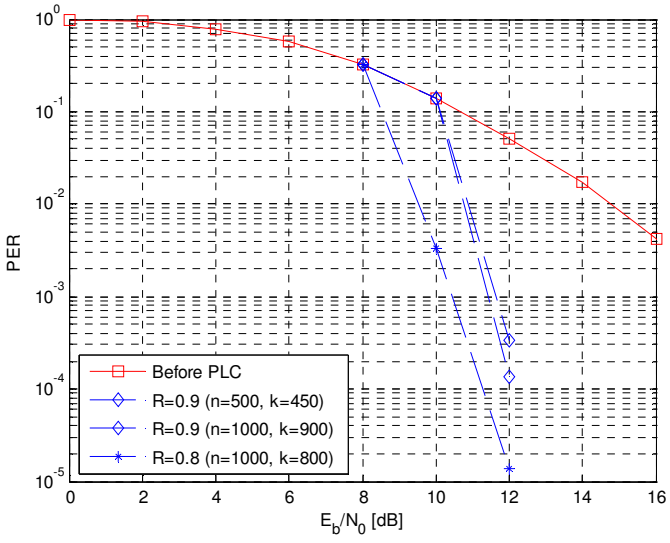

Figure 33: Performance of AeroMACS with the proposed PLC in the NLOS scenario.

The best performance is obtained in correspondence of the higher block length values and in particular for the case with rate 0.8, that beneficiates of more redundancy. The values of n corresponding to 1000

packets provide better results with respect to the case with n=500; in fact, here, the encoding is performed over a larger time period, providing the possibility to compensate better the slow fading. However, a coding block of 1000 packets introduces a latency of almost 5 s, corresponding to the double of the delay introduced by a block of 500 packets (latency of almost 2.5 m). Therefore, for a given coding rate, high performances have to deal with higher delays.

In all the cases, the performance provided by the cases with PLC introduces large performance gains to the performance of AeroMACS. Already the case with packet-level code (n=500, k=450), which is outperformed by the other two cases, for a PER=10^{-2} offers a gain of almost 4 dB.

4.2 Cooperative Techniques

One possibility to enhance the performance of AeroMACS is the application of spatial diversity techniques. MIMO techniques represent a straightforward way to realize it, and their advantages have been widely acknowledged. However, in the aeronautical domain, the introduction of multiple-antenna systems, especially on-board aircraft, is seen to be critical, limiting the applicability of MIMO. Cooperative communication techniques can represent a valid alternative, since they allow single antenna systems to exploit spatial diversity [COV79, LAN01, LAN03, SED03, SED03b, ZAH03]. Cooperative communications represent a new paradigm based on the utilization of heterogeneous resources in order to increase the overall performance of the system. A virtual antenna array may be created by the combination of antennas of different users, obtaining spatial diversity. The classic relay system can be seen as an example of cooperative communication, where a user of the system acts as a relay forwarding the received signal. However, cooperative communication methods include more possibilities. There are several fashions for cooperating and the "helping" user may elaborate the received signal in many different ways.

In this section, we analyze low-complexity cooperative communications protocols in the context of AeroMACS. Detect and forward, amplify and forward and coded cooperation methods are investigated, analyzing their properties in the aeronautical context. We illustrate the realization of two simple cooperative communication schemes for improving the performance of AeroMACS in the RL. The proposed scheme, based on the amplify and forward method (AF), increases the reliability of the system by means of a relay which simply forwards the source signal to the destination. In our investigation, the relay can be an aircraft (in this way, the introduction of a new relay network is avoided), but also a separate "relay entity". The resulting system can beneficiate of a spatial diversity of order two, which is equivalent to the result obtained with a multiple-antenna system with two antennas. The receiver can perform a simple selection combining of the two received signals or can adopt a more sophisticated algorithm (e.g. maximal ratio combining), which allows exploiting all the received power. However, in order to perform MRC, all the channel components must be known. Hence, it is necessary to estimate not only the resulting channel coming from the combination of the route source-relay-destination, but also the channel relative to the segment relay-destination. In order to properly estimate all the channels, we insert some pilot tones at the

relay before amplifying the signal, allowing the destination to coherently sum all the received signals and maximize the performance.

A new cooperative scheme which provides a solution to the typical efficiency reduction related to the distributed diversity is introduced in [PUL12] [PUL12s][PUT12]. High system efficiency is reached, while offering diversity two to the most important part of the message.

4.2.1 Overview of Cooperative Communications

In a cooperative communication system, the transmission between the source and the destination is helped by one (or more) partner, which receives the transmitted signal and retransmits to the destination a copy of the signal transmitted by the source. In this way, a distributed MIMO network is created and a diversity gain is obtained.

In a multi-user system, the users can act as cooperating partners creating a cooperative network. Sharing their resources, they obtain better global performance. Moreover, they keep the costs low, since the installation of an ad-hoc relay network is avoided. This solution offers the advantage of flexibility, large number of potential cooperative partners and operational efficiency. The vehicles operating on the airport surface offer furthermore sufficient power for performing rather complex operations. Again, the cooperation among users offers a wide availability of potential terminals out of which choosing the most appropriate relay (i.e. the one located in the best position with respect to the source and the destination terminals).

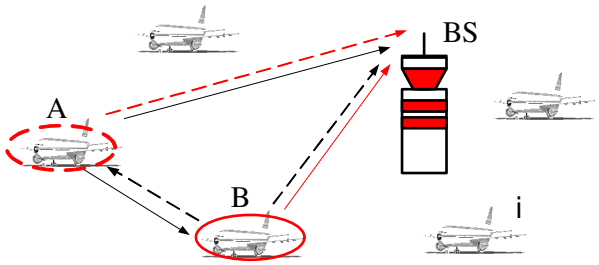

Figure 34: Scheme of cooperation between aircrafts.

Figure 34 represents a scheme of cooperative communication where the users A and B collaborate. In the first case (continuous lines), the user A is helped in the communication with the base station by the user B (red line). Here A is the source terminal and B acts as relay transmitting to the base station a replica of the signal transmitted by A. However, the roles can be exchanged and the user A can become the cooperative-terminal that helps B (dotted lines). In this example the users A and B cooperate with each other. Though, the cooperation can take place not only with cooperating couples of users, the partner assignation can be made in several ways according to different algorithms.

The relay terminal transmits a replica of the signal transmitted by the users according to a certain cooperation method. There are different cooperation techniques characterized by different complexity,

modifications required to the system and performance. However, all the methods require the receiver separating the original signal from its replicas. The easier way to obtain this separation is to adopt time division, letting source and relay transmitting in different time slots. Table 5 describes an example of single-relay transmission using time division. In the first time slot (t_1), the source transmits while destination and relay receive. Then, during the second time slot (t_2), the relay transmits and the destination receives.

Table 5: Cooperation based on time-division

	(t_1)	**(t_2)**
Source	Tx	Inactive
Relay	Rx	Tx
Destination	Rx	Rx

4.2.1.1 *Amplify and Forward*

Amplify and forward (AF) methods have been proposed by Laneman in **Error! Reference source not found.** [LAN03] and constitute the simplest form of cooperation between systems. In this case, the relay system only amplifies and retransmits the noisy version of the signal received from the source. The base station receives the different versions of the signal and exploits them for improving the detection of the transmitted bits. Although the noise at the relays is amplified by the cooperation, the system receives independent replicas of the signals increasing the system diversity. For a system with two user cooperating (for example a system with a single relay), a diversity of order two is achieved. Hence, full diversity is attained.

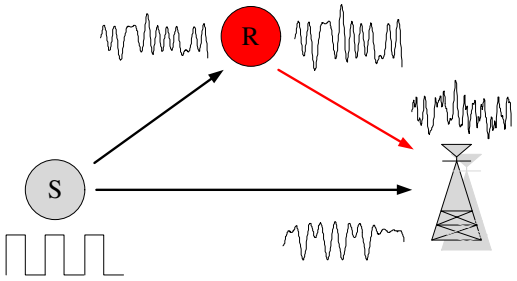

Figure 35: Amplify and forward scheme.

4.2.1.2 *Decode and Forward*

Within the cooperative communication methods, decode and forward (DF) is the one closest to the initial idea of relay system. As represented in Figure 36, the relay detects, decodes and retransmits the signal transmitted by the source. Sedonaris in **Error! Reference source not found. Error! Reference source not found.** proposed one of the first example of DF, with decode-and-forward cooperation made by code-division multiple access (CDMA). In DF, as illustrated in Figure 36, the relay decodes the source's signal and retransmits it after re-encoding the information. The destination receives two independent replicas of the

signal that exploits for extracting the information bits. Differently from the previous method, the receiver doesn't require to know the channel between S and R to perform a coherent combination of the signals (only the channels between R-S and S-D are required, indeed).

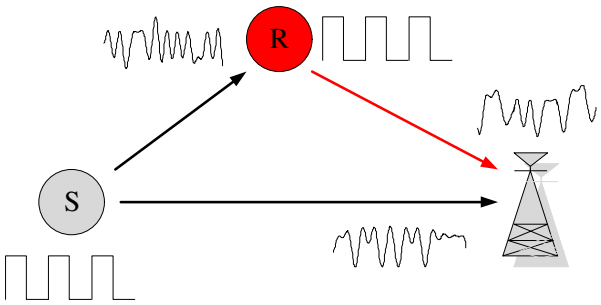

Figure 36: Decode and forward scheme.

4.2.1.3 *Coded Cooperation*

Coded cooperation **Error! Reference source not found. Error! Reference source not found.** combines channel coding with cooperation, creating a distributed coding. The basic idea is that each partner transmits a portion of the code, increasing the redundancy. Figure 37 shows a scheme of coding cooperation between two users. Each user encodes their information (the bits of the user A are represented in grey in the figure while the ones of the user B in red) and then divides the codeword into two subsets containing N_1 and N_2 bits, respectively. The first subset is transmitted by the original user in the first frame. After decoding the first subset, the collaborating-user can obtain the second subset of the partner and transmits during the second frame. The receiver combines the fragments received by the collaborating partners and decodes them jointly obtaining the information bits. Again, including a cyclic redundancy check (CRC) code on the sub-messages, the partners can independently decide to transmit the second subset of the own message in place of the partner's. In this way, whenever the link between the partners were bad (not allowing a proper decoding and retransmission of the message) the user decides to entirely exploit its resources for itself. Thus, in this case, the system acts as non-cooperative. The partners are hence able to decide whenever it is convenient cooperating or not (this decision can be autonomous between partners; indeed the "cooperation mode" doesn't require a centralized decision system). This method represents an attractive cooperation option, thus it achieves gains, while preserving information rate, transmit power, and bandwidth of the non-cooperative system.

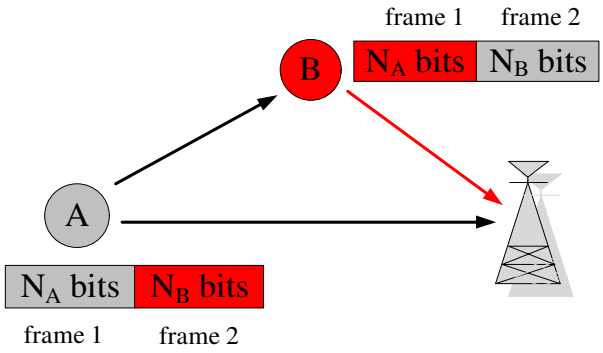

Figure 37: Coded cooperation scheme.

4.2.2 Cooperation in the Airport Environment (AeroMACS)

In a multi-user system, the users can act as cooperating partners in order to share resources and obtain better information transmissions. The creation of a cooperative network represents a convenient option for a multi-user system. In this case in fact, the installation of an expensive ad hoc relay network is avoided. Besides, the system users offer the great advantage of having already integrated all the devices necessary for transmitting and receiving signals. Hence, different types of cooperation algorithms are implicitly allowed. Again, the cooperation among users offers a large range of available terminals within choosing the most appropriate relay.

AeroMACS beneficiates of a large population of aircraft and represents a good candidate for the use of cooperative communications.

Within the airport network, the aircraft could cooperate with each other increasing the performance of the system. The large population of aircraft could offer a wide range of potential relays, out of which choosing in a real time fashion the best one.

At the airport, the ideal application scenario for cooperative communications is represented by the parking scenario. In fact, in this case the aircraft is often in non-line-of-sight with the control tower and the performance of the system tends to suffer for limited time and frequency diversity. Moreover, the network topology (including aircraft and control tower) is static, allowing reliable estimations of the relevant channel gains. Hence, the application of cooperative communications could largely improve the quality of the transmission.

The best cooperating condition is represented by a relay whose link towards the destination presents a better SNR with respect to the one provided by the direct link between source and destination. Such situation may be represented by a relay in line of sight with the user and eventually also with the control

tower (and hence with a high SNR in correspondence of both the S-R and R-D links, as depicted in Figure

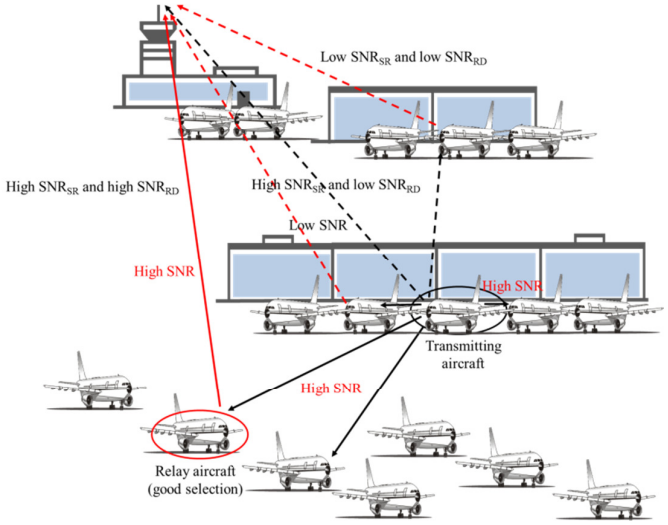

38

Figure 38).

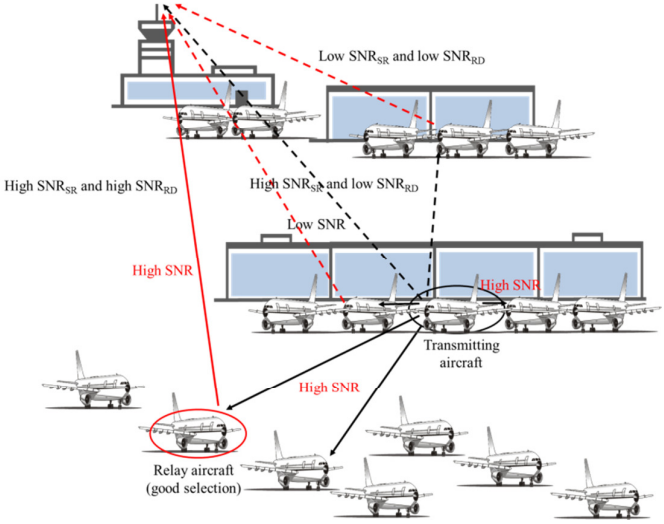

Figure 38: Cooperation between aircraft at the airport.

In order to select the most appropriate aircraft-relay, the user could (independently from the control tower) exchange messages with the potential relays. Besides, it is possible to exploit the characteristics of the airport topology. Since the airport vehicles are parked according to a specific scheme, this could be used to simply select a good relay. In fact, aircraft parked close to each other guarantee a link between them with high SNR. Hence, it is possible to group potential cooperating-aircraft a priori and then, the active user can independently choose a relay between the group's partners. The selection of the relay can also be done in a completely centralized way. In this case the base station can decide which users cooperate. The centralization of the cooperation increases the network overhead and the complexity.

The cooperative methods presented in the previous section assume that the original and the relay signals are transmitted orthogonally, hence, that the base station is able to separate them. However, except in **Error! Reference source not found.**, where the separation of the signals is performed by CDMA, the division of the signals represents a critical aspect. The easiest way to separate the signals is time division (see Table 5), that distributes the source and relay transmissions in different time interval. Another method is frequency-division. Though, many systems use different bandwidths for receiving and transmitting, making difficult the implementation of cooperation without changing the hardware.

AeroMACS is a system based on OFDMA which will operate in TDD mode. Although the frame is divided in forward link (FL) and reverse link (RL) sub-frames, the ratio between FL and RL is variable, therefore, the relay can receive even during the RL. AeroMACS provides multiple chances of cooperation by means of time division, OFDMA sub-channel and even frequency sub-channel. In the first case, the relay could transmit in a different frame but over the same OFDMA sub-channel used by the source message. Moreover, the relay has also the possibility to transmit over a different OFDMA sub-channel.

4.2.3 AF Implementation for AeroMACS

We implemented an AF scheme to the AeroMACS system. We considered a single relay system, where an aircraft (partner aircraft) acts as a relay receiving and retransmitting the user's signal.

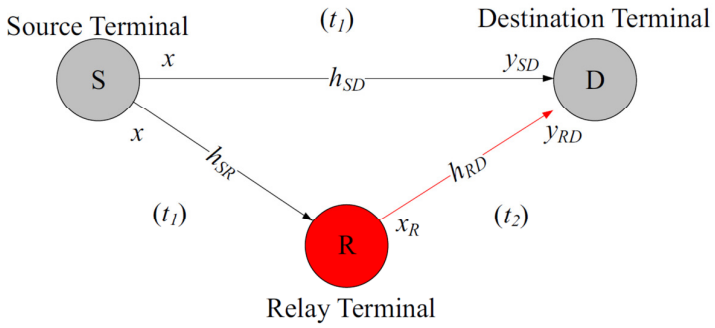

Figure 39: Scheme of a single relay system.

Figure 39 represents a basic amplify and forward scheme, where the communication between a source (S) and a destination (D) is helped by a single relay (R). The relay receives the signal transmitted by the source and retransmits it after an amplification defined by a factor *C*. Assuming the source transmitting only during the first slot, and the relay transmitting on the second slot, the destination receives the signals y_{SD} and y_{RD} during the first and the second slot, respectively. The system may be thus modeled as

$$\begin{cases} y_{SD} = h_{SD}x + n_{SD} \\ y_{SR} = h_{SR}x + n_{SR} \\ y_{RD} = h_{RD}x_R + n_{RD} \end{cases} \quad (4.1)$$

where x represents the transmitted signal at the source, h_{SD}, h_{SR} and h_{RD} are the fading coefficients corresponding to the source-destination, S-R and R-D links, respectively. The signal retransmitted by the relay x_R is the received version of x amplified by a factor C ($x_R=C(x\,h_{SR}+n_R)$). It is convenient to call $y_1=y_{SD}$ and $y_2 = y_{RD}$ and rewriting the previous equation as:

$$\begin{cases} y_1 = h_1 x + n_1 \\ y_2 = h_2 x + n_2 \end{cases}, \tag{4.2}$$

letting the indexes 1 and 2 represent the direct path S-D and the one provided by the relay S-R-D, respectively. Hence, the signal forwarded by the relay sees a channel $h_2= C\,h_{SR}h_{RD}$, and a noise $n_2= Ch_{RD}n_R+n_{RD}$. All the noise components are modeled as complex Gaussian random variables with zero mean and variances $\sigma_{SD}^2= \sigma_1^2$, σ_{SR}^2 and σ_{RD}^2 ($n_{SD} \sim N(0; \sigma_{SD}^2)$; $n_{SR} \sim N(0; \sigma_{SR}^2)$; $n_{RD} \sim N(0; \sigma_{RD}^2)$). Normalizing the two signals by the relative noise variance[13] σ_1^2 and σ_2^2, it is possible to obtain two signals $\dot{y}_1$ and $\dot{y}_2$ with the same noise variance equal to 1 ($\dot{n}_1$, $\dot{n}_2 \sim N(0; 1)$).

$$\begin{cases} \dot{y}_1 = \dfrac{y_1}{\sigma_1} = \dot{h}_1 x + \dot{n}_1 = \dfrac{h_1}{\sigma_1}\cdot x + \dfrac{n_1}{\sigma_1} \\ \dot{y}_2 = \dfrac{y_2}{\sigma_2} = \dot{h}_2 x + \dot{n}_2 = \dfrac{h_2}{\sigma_2}\cdot x + \dfrac{n_2}{\sigma_2} \end{cases} \tag{4.3}$$

The system described by the previous equation is equivalent to a generic 1x2 single input multiple output (SIMO) system, hence, since the optimum

weights of the maximum ratio combining (MRC) receiver are given by $w_1 = \dot{h}_1^*$ and $w_2 = \dot{h}_2^*$ (as for a 1x2 MRC system case). The resulting signal u, obtained by the combination of the two received signals y_{SD} and y_{RD}, becomes:

$$u = \dot{h}_1^* \cdot \dot{y}_1 + \dot{h}_2^* \cdot \dot{y}_2 = \frac{h_1^*}{\sigma_1^2}\cdot y_1 + \frac{h_2^*}{\sigma_1^2}\cdot y_2 \,, \tag{4.4}$$

that can be rewritten as

$$u = \left(\frac{|h_1|^2}{\sigma_1^2} + \frac{|h_2|^2}{\sigma_1^2}\right)\cdot x + \frac{h_1^* n_1}{\sigma_1^2} + \frac{h_2^* n_2}{\sigma_1^2} = h_{tot}\cdot x + n_{tot} \tag{4.5}$$

$$n_{tot} = \frac{h_1^* n_1}{\sigma_1^2} + \frac{h_2^* n_2}{\sigma_1^2} \tag{4.6}$$

$$\sigma_{n_{tot}}^2 = E\{|n_{tot}|^2\} = \\ = \frac{|h_1|^2}{\sigma_1^2} + \frac{|h_2|^2\,\sigma_{RD}^2}{\sigma_2^4} + \frac{|h_2|^2\,C^2\,|h_{RD}|^2\,\sigma_R^2}{\sigma_2^4} \tag{4.7}$$

[13] Note that if we assume the noise variance for all the systems identical and equal to σ^2 ($\sigma_{SD}=\sigma_{RD}=\sigma_R=\sigma$), the variances relative to the two paths become $\sigma_1^2=\sigma_{SD}^2=\sigma^2$ and $\sigma_2^2= \sigma^2 (C^2\,|h_{RD}|^2+1)$.

$$\sigma^2_{n_{tot}} = \frac{|h_1|^2}{\sigma_1^2} + \frac{|h_2|^2}{\sigma_2^2} \tag{4.8}$$

Assuming the signal x uniformly distributed with mean power equal to 1 ($E\{|x|^2\}=1$), the total instantaneous signal-to-noise ratio γ_{tot} becomes:

$$\gamma_{tot} = \left(\frac{|h_1|^2}{\sigma_1^2} + \frac{|h_2|^2}{\sigma_2^2} \right) = \gamma_1 + \gamma_2 \tag{4.9}$$

[14]

$$\gamma_{tot} = \frac{1}{\sigma^2} \left(|h_{SD}|^2 + \frac{|h_{SR}|^2 |h_{RD}|^2}{\left(|h_{RD}|^2 + \frac{1}{C^2} \right)} \right) = \gamma_{SD} + \gamma_{SRD} \tag{4.10}$$

.

Hence, at the receiver the resulting instantaneous γ_{tot} is the sum of the two γs relative to the different paths. The first term represents the γ relative to the direct link between the source and the destination and corresponds to the performance offered by a single antenna system with no relay. The second term of the equation describes the signal to noise ratio corresponding to the link source-relay-destination and represents the gain, in term of signal-to-noise ratio, introduced by the relay. Focusing on γ_2

$$\gamma_2 = \frac{1}{\sigma_2} \left(\frac{|h_{SR}|^2 |h_{RD}|^2}{|h_{RD}|^2 + 1/C^2} \right), \tag{4.11}$$

we observe that for high values of C the equation (4.11) becomes the signal to noise ratio corresponding to the S-R link γ_{SR}. Hence, the system behaves as a multiple antenna system with two receiving antennas[15]. Vice versa, for $C= 0$, $\gamma_2= 0$ and the system converts to a non-cooperating system. For $C=1$, as it is reasonable to assume, γ_2 becomes:

$$\gamma_2 = \frac{1}{\sigma_2} \left(\frac{|h_{SR}|^2 |h_{RD}|^2}{|h_{RD}|^2 + 1} \right). \tag{4.12}$$

From the previous formula it is clear to see that it is important to have the γ relative to the link between the source and the relay (γ_{SR}) high. It is trivial to understand that a high γ_2 is fundamental for a good cooperation and to improve the performance of the system. However, as discussed in the previous section, it is possible to adopt some criteria in the relay selection in order to satisfy this request.

[14] This result is equal to the one provided by a 1x2 MRC system.

[15] Note that we are neglecting the power used by the relay for retransmitting the source's information. Since C is directly related to the relay power consumption, in a real system, high values of C are unfeasible.

4.2.3.1 *On the Channel Estimation*

The previous analysis of the generic amplify and forward system shows that a coherent receiver requires to know all the three different channels (hence, the ones relative to the links S-D, S-R and R-D). In order to properly estimate all the channels, the relay could add some pilot tones, according to the scheme illustrated in Figure 40. In this case, the reverse link of the WiMAX standard is considered. Hence, the frame and the pilot tones positions are based on the tile concept. The frame is divided in tiles, which consist of blocks of 12 subcarriers with pilot sub-carriers at the edges (as illustrated in Figure 40). The relay inserts two pilot values in correspondence of the first two pilots of the tile (the ones on the first frequency line) and modify the frame according to scheme presented in the figure. If the channel is sufficiently slow in time, the destination is able to estimate all the channels.

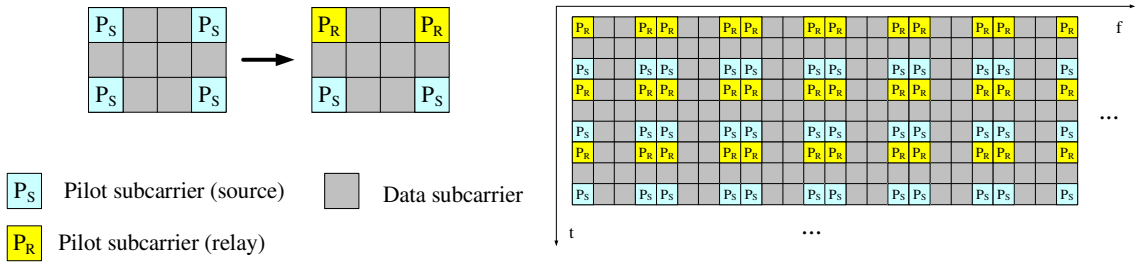

(a) Tile scheme. **(b) Frame scheme.**

Figure 40: Tile (a) and frame (b) schemes of the pilot tones introduction at the relay.

In this case, the receiver may perform the channel estimation only in frequency direction, using the two pilots assigned to the link and assuming the channel constant over three consecutive OFDM symbols. The pilots inserted by the relay (PR) to estimate the R-D channel and the pilots of the source (PS) to estimate h_2.

4.2.3.2 *Performance Results*

We analyzed performance of the described scheme in the context of AeroMACS and in particular on the reverse link case. For our simulations we used convolutional coding with rate 1/2 and QPSK subcarrier modulation. We considered ideal channel estimation (ID) and linear interpolation based on the pilot tones and tailored for the WiMAX tile structure. Table 6 describes the relay simulation scenarios, i.e. the links between source and destination, source and relay and relay and destination. Our analysis is focused on the parking situation[16], which corresponds to the most critical scenario. Since we account line-of-sight and non-line-of-sight situations between the communicating entities, the Rice factor values are equivalent to 0 or 20 dB.

Table 7 summarizes the main system parameters used in the simulations.

[16] The parking scenario is mainly characterized by NON line of sight and limited mobility; detailed parameters of this scenario can be found in [PUL10a] and [LIV11b].

Table 6: Relay simulation scenarios

Simulation scenario	Case 1	Case 2	Case 3
Channel scenario h_{SD}	PARKING	PARKING	PARKING
K_{SD} [dB]	0	0	0
Channel scenario h_{SR}	PARKING	PARKING	PARKING
K_{SR} [dB]	20	20	0
Channel scenario h_{RD}	PARKING	PARKING	PARKING
K_{RD} [dB]	0	20	0

Table 7: Simulation parameters

Parameters	Value
Link	RL
Bandwidth	5 MHz
FFT size	512
Symbol time TS (w/o CP)	102.4 µs
CP	1/8TS
Subcarrier spacing Δf	10.94 kHz
Coding, rate	Convolutional, 1/2
Decoding	Soft Viterbi
Modulation	QPSK
Channel estimation	ID, LIN (freq. domain)
Relay Amplification Factor C	1, 10, 50

Finally, we illustrate the results obtained by simulations applying the above described scheme to AeroMACS. The first figures show the performance of the system in term of bit error rate versus average E_b/N_0 over the link SD[17]. Figure 41 (left) depicts the performance of a generic single relay amplify and forward system in the AeroMACS context for the third relay links configuration case. Here, the channels between the three communicating entities are assumed equal to the parking scenario and statistically independent. Therefore, the link offered by the relay doesn't provide a better SNR but only a diversity gain. The figure shows the performance with ideal channel estimation and different amplification factors. Three different relay amplification factors are showed for analyzing the system behavior. High values of C are considered as reference case, although they are unrealistic and do not lead to a fair comparison[18]. All the cooperative configurations provide a large performance improvement with respect to the non-cooperative case which is

[17] The power used for the relay transmission is not accounted in these figures. However, for a fair comparison it is necessary to account that the total power used for the cooperative transmission is increased with respect to the NON-cooperative system.

[18] In this work the performance of the system is shown per the link S-D, indeed. The power used by the relay for helping the user transmission is neglected. However, the total system power shall be controlled and the increase of C should be avoided.

represented by the black line (C=0). The cases with high C provides better performance, gaining almost 2 dB with respect to the case with C=1. In fact, as showed in the previous section, increasing the C value, the system becomes equivalent to a single input multiple output system with two antennas and MRC receiver. Indeed, the performance of the cooperative system is equal to the one provided by the 2×1 MRC system. The gains provided by the cooperative schemes are remarkable. Gaining a diversity order equal to 2, they double the slope of the non-cooperative curve (exactly as the multi-antenna case).

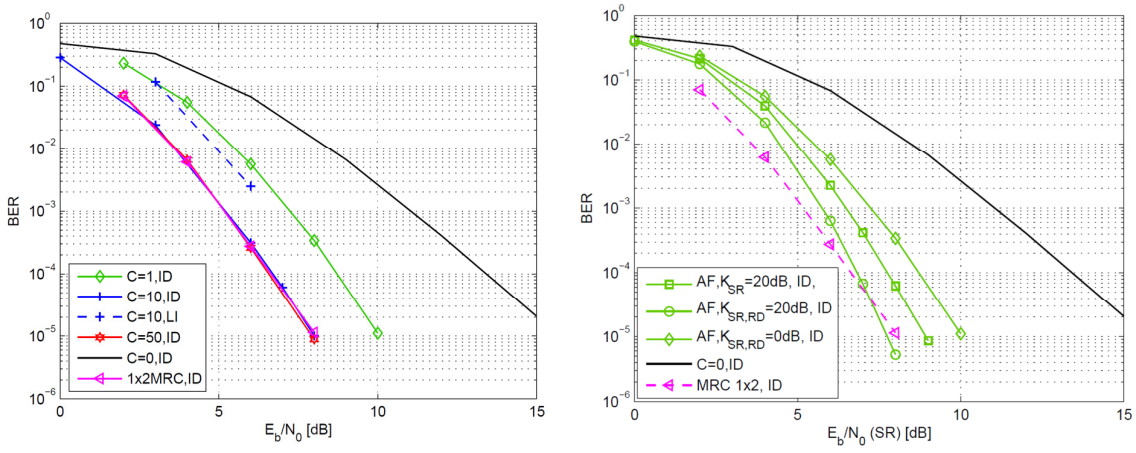

Figure 41: Performance of AeroMACS with AF scheme. Performance of the system for the third simulation scenario using different relay amplification factor C, and ideal channel estimation (left). Performance of AeroMACS with AF scheme and different relay links conditions, C=1, and ideal channel estimation (right).

Figure 41 (right) provides the performance of the system for different cooperation conditions (i.e. different channels between source, relay and destination). Perfect channel knowledge and relay amplification factor C equal to 1 are assumed. Besides the worst case (third scenario indicated by the green curve with diamond marker) considered in the previous figure, two scenarios with different relay links conditions and hence different Rice factor K are considered. The curve with square markers represents the first simulation case, where the source and the relay are in line-of-sight (K_{SR}= 20 dB). The channel between relay and destination preserves a low Rice factor K_{RD}= 0 dB (as the one between S and D). The second simulation case (curve with round markers) presents high Rice factor value for both the links (K_{SR}= K_{RD}= 20 dB), as the relay is assumed in line-of-sight with source and destination, both. All the cooperation cases provide large performance gains with respect to the non-cooperative case (black curve).

Figure 42 shows the performance of the system with the proposed way to perform real channel estimation for all the channel coefficients and the third simulation scenario. We used linear channel interpolation based on the pilot tones. The interpolation, done in the frequency domain, is performed in time and frequency direction for the non-cooperative case and only in frequency direction (as described in the previous section) for the cooperative case. The real channel estimation cases (indicated with LI) are represented by dashed

lines, while the ideal channel knowledge ones (ID) with continuous lines. The introduction of imperfect channel estimation produces a loss of almost 1.6 dB on the system performance.

In order to provide a fair performance evaluation of the AF scheme in the AeroMACS context, we include the behavior of the BER at the variance of the total energy per bit used by the system for the transmission (E_{tot}= Eb_{Source} + Eb_{Relay}). The following figures illustrate the performance in terms of BER versus Eb_{tot}. Figure 43 (left) represents the results obtained for the worst case, i.e. the links S−R and R−D are not reliable with K= 0 dB. Figure 43 (right) compares the performance obtained with different conditions of the relay links.

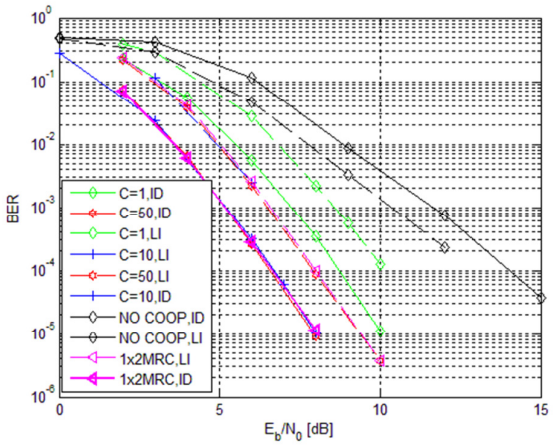

Figure 42: Performance of AeroMACS with AF scheme using ideal channel estimation and the proposed linear interpolation algorithm.

From these figures it is clear that the use of the relay increases the total power spent by the system. Hence, certain values of the amplification factor C are completely unfeasible (as C= 10 and C= 50, respectively represented by the blue and red curves in Figure 43 (left)). Considering the total energy of the system, all the relay curves appear shifted to the right with respect to the previous figures. However, the slope is identical and the performance improvement still present. For the case with C= 1, the curve is shifted of almost 3 dB with respect to Figure 41. This implies that at BER=10^{-4} the performance gain is almost 2 dB for the worst case (K_{SR}= K_{RD}= 0 dB), 3 dB for the scenario with reliable link between the source and the relay (K_{SR}= 20 dB, K_{RD}= 0), and 4 dB for the best case (K_{SR}= K_{RD}= 20 dB).

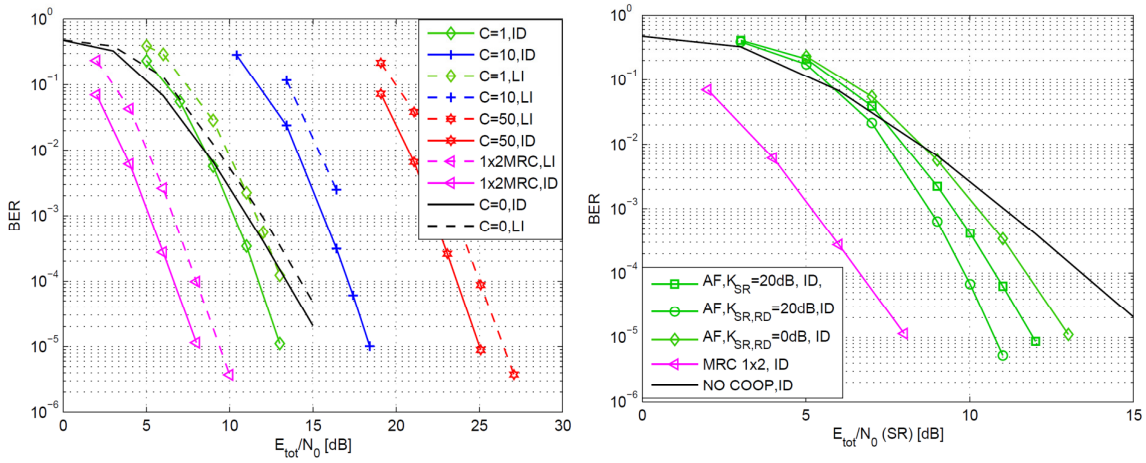

Figure 43: Performance of AeroMACS with the AF scheme considering the total energy per bit E_{tot}. Evaluation of the impact of the amplification factor C (left). Performance with different different Rice factor K for the relay links, C=1, and ideal channel estimation (right).

4.2.4 DF Implementation for AeroMACS

Hereafter, we implemented a DF scheme with a single relay for the RL of the AeroMACS system. Again, we assume the relay being an aircraft and we use the two times transmission scheme described by Table 5. Considering the communication scheme represented in Figure 39, the control tower receives two signals during two different time slots. With respect to the previous case, the relay doesn't amplifies the source's signal but decodes, re-encodes and retransmits it. We can describe the system with the following equations where the signal transmitted by the source and the relay are indicated with x_R and x, respectively,

$$\begin{cases} y_{SD} = h_{SD}x + n_{SD} \\ y_{SR} = h_{SR}x + n_{SR} \\ y_{RD} = h_{RD}x_R + n_{RD} \end{cases} \quad (4.13)$$

x_R represents the received signal (h*x) decoded and re-encoded and we can practically indicate it with . Hence, if the relay can properly decode the transmitted signal, the destination will receive a useful replica of the signal. Vice versa, if the relay cannot decode the signal the destination will receive a not reliable replica of the signal. Assuming the channel between source and relay reliable (i.e with high *K* factor), the behavior of the system becomes equivalent to a SIMO system. Utilizing a MRC receiver, we can maximize the total SNR_{tot} of the system. As consequence of the reliability of h_{SR}, we write $x_R =$ ≈ x. Hence, we can write the two received signals y_{SD} and y_{RD} as

$$\begin{cases} y_{SD} = h_{SD}x + n_{SD} \\ y_{RD} = h_{RD}x + n_{RD} \end{cases} \quad (4.14)$$

This equation is equivalent to the MRC system with two receiving antennas, hence the receiver works exactly in the same way of one of a MIMO system 1x2. Hence, the total received signal u is again obtained as

$$u = y_{SD} * y_{SD}^{*} + y_{RD} * y_{RD}^{*} \tag{4.15}$$

The total SNR_{tot} is therefore given by the sum of the two SNRs relative to the direct path (SNR_{SD}) and the relay component (SNR_{RD})

$$SNR_{tot} = \frac{E\{|x|^2\}}{\sigma^2}\left(|h_{SD}|^2 + |h_{RD}|^2\right). \tag{4.16}$$

4.2.4.1 *Simulation Results*

Simulation Parameters

For our simulations we used the system parameters summarized in Table 8. We adopted the channel model described in [PUL10a, LIV11b] with three different relay simulation scenarios, as summarized in Table 9. The first scenario reproduces the case where a reliable channel is available between the source and the relay (h_{SR}), while the other links (S–D and R–D) are typical parking scenarios with NLOS conditions. The second simulation scenario represents a situation where the relay has not only a good h_{SR} but also a good h_{RD}. This case is obviously the ideal scenario; here, the link provided by the relay outperforms the direct path. The third case constitutes the worst case, where the link provided by the relay is equivalent to the direct one. In all the cases, we assumed the typical parameters of the parking scenario, except the Rice factor K that can be either 0 dB or 20 dB.

Table 8: Simulation parameters

Parameters	Value
Link	RL
Bandwidth/ FFT size	5 MHz/ 512
Symbol time TS (w/o CP)	102.4 μs
CP	1/8TS
Subcarrier spacing Δf	10.94 kHz
Coding, rate	Convolutional, 1/2
Decoding	Soft Viterbi
Modulation	QPSK
Channel estimation	ID, LI (freq. domain)

Table 9: Relay simulation scenarios

Simulation scenario	Case 1	Case 2	Case 3
Channel scenario h_{SD}	PARKING	PARKING	PARKING
K_{SD} [dB]	0	0	0

Channel scenario h_{SR}	PARKING	PARKING	PARKING
K_{SR} [dB]	20	20	0
Channel scenario h_{RD}	PARKING	PARKING	PARKING
K_{DR} [dB]	0	20	0

Figure 44 (left) shows the performance of the system with the introduction of a DF scheme. We considered three different simulation scenarios and perfect channel knowledge. The first case represents the situation with relay in LOS with the source but no with the destination. This case (represented by the purple curve with square markers in the figure) is the most realistic and interesting, since in the airport parking context this condition is simple to acquire. The case 2 (K_{SR}= K_{RD}= 20 dB, curve with round) represents the best cooperation scenario where the relay is in LOS with source and destination both. Here, the link provided by the relay is better than the direct one, and, the communication could stand only on the relay link. The case 3 (K_{SR} = K_{RD} = 0 dB, curve with diamond marker) foresees an unlucky situation with relay in NLOS with both source and destination. In this case, the condition of reliable channel between source and relay falls. Hence, the cooperation is ineffective. Since the link between source and relay isn't completely unreliable the performance is comparable to the one of the non cooperative system. However, in this context, it is preferable not to cooperate or, eventually, switching to an AF scheme. Figure 44 (right) shows the results obtained with DF accounting linear channel interpolation. Figure 45 illustrates a comparison between the performance provided by AF (green curves) and DF (purple curves). The simulation results reflect the theoretical behavior. As expected, for a "not very reliable" channel between source and relay, the results of AF (green curve with diamond marker) outperform the ones offered by DF (purple curves with diamond marker). The behavior changes with reliable h_{SR}, characterized by high K= 20 dB (curves with square and round markers); here, the performance of DF outperforms AF, since in this case the noise introduced at the relay is compensated. In order to obtain a comprehensive evaluation of the use of the relay scheme, we include also the results in terms of BER versus the total energy per bit used by the system. Figure 46 (left) shows the performance of the system with a relay DF scheme, while Figure 46 (right) compares the results obtained with AF and DF. Similarly to the AF case, these curves are shifted on the right of almost 3 dB with respect to Figure 44 (left) and Figure 45. Thus, the gain introduced by the relay appears for higher SNRs.

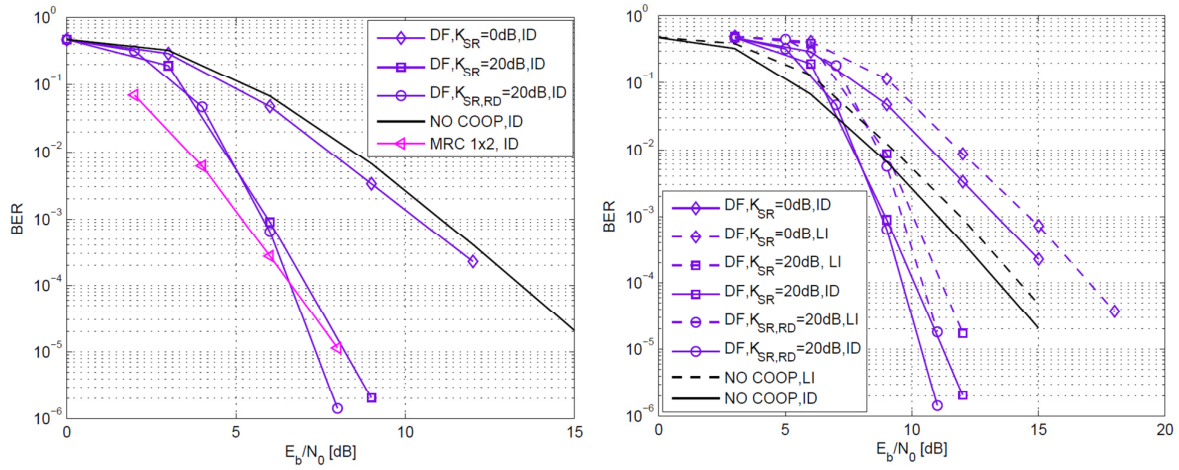

Figure 44: Performance of AeroMACS with DF scheme, ideal channel estimation (left). Performance of AeroMACS with DF scheme, linear pilot interpolation (right).

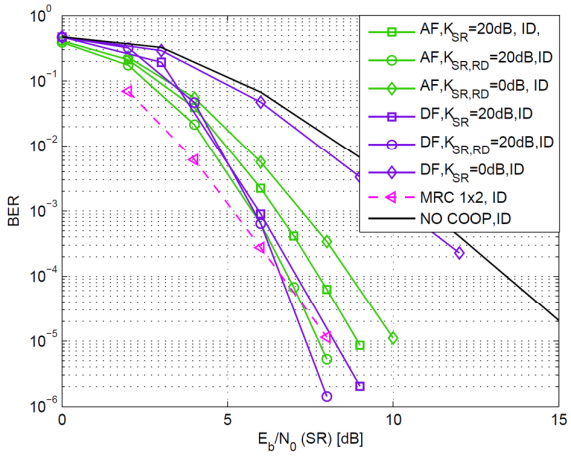

Figure 45: Comparison between the performance provided by AF and DF, linear pilot interpolation (left).

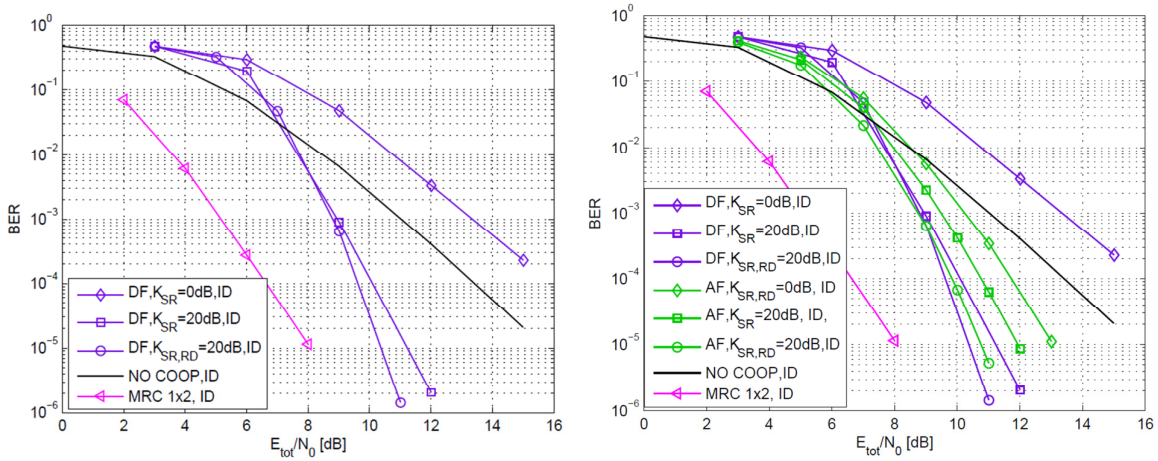

Figure 46: Performance of AeroMACS with DF scheme considering the total energy per bit and different Rice factor K for the relay links (ideal channel estimation.) (left). Comparison between AF and DF as function of E_{tot} (right).

4.3 Summary

In this Section, we analyzed potential solutions for enhancing the performance of AeroMACS. Since the performance of the system shows degradation in correspondence of the scenarios characterized by NLOS condition with the control tower, moderate or no mobility, and lack of diversity, we investigated potential methods for increasing the diversity of the system, and thus improving its performance. We analyzed techniques as packet level coding and cooperative communications. The first method is based on time diversity, while the second one is based spatial diversity (or cooperation diversity).

All the investigated methods provide large performance gains, and hence, represent appealing solutions. Though, they require different modifications to the base system, and therefore, constitute interesting candidates for different phases of the AeroMACS upgrade plan. We summarize next the main outcomes of our analysis, including pros and cons of each technique in the context of the airport communications.

Packet Level Coding Packet level coding represents a simple yet effective mean to cope with slow-fading channels. Since a packet level code operates on symbols that are (in general) packets of fixed size, the packet-level coding sub-layer can be introduced on the higher layers of the protocol stack (e.g., at the application layer), rendering the introduction of packet-level coding almost transparent to the rest of the communication stack. Additionally, the inherent low complexity of erasure decoding allows implementing the packet-level encoders and decoders via simple software routines running on general purpose computing platforms. By this way, data rates of several hundred Mbps can be achieved. Thus, packet level coding is indeed a very-low complexity upgrade, which can be introduced in the system even after deploying the hardware infrastructure. As an added value, packet-level coding can be easily integrated with hybrid ARQ protocols by means of the fountain coding concept, allowing the delivery of broadcast content with nearly-optimum exploitation of the down link bandwidth. Packet level coding is especially efficient when the large blocks of data are processed by the packet level encoder. More specifically, the encoded blocks shall be longer than a few channel coherence times to enjoy sufficient diversity. As a result, depending on the channel coherence time, large latencies may be expected. Thus, packet-level coding is not suitable for delay-critical services (such as voice communications). However, in many applications (e.g., file delivery), delays are indeed not a problem and this technique represents an excellent solution.

Cooperative Techniques Cooperative communications provide spatial diversity, or more specifically cooperation diversity, even for single-antenna systems. They hence represent a potential solution for cases where the use of multiple antennas is not allowed (e.g. on the aircraft). The cooperation between users has a great potential in the airport context. The large population of aircrafts offers a large number of potential partners. Moreover, the aircrafts are provided with a large power supply, offering the possibility to perform even rather complex operations as coding, decoding, modulation, etc. Among the cooperation schemes, even the simpler ones, as amplify and forward and decode and forward, are able to provide large performance enhancements. More specifically, for the single-relay case, they are both able to attain a diversity of order two. This diversity order is the maximum achievable with a single relay, and is the same provided by a multiple antennas system with two antennas. Assuming the channel between the source and the relay as reliable, DF provides better performance than AF. In this condition, the relay system becomes equivalent to a 2×1 STC, providing basically the same performance. Although less performing, AF is more robust with respect to the channel condition on the source-relay link.

Albeit simple, these schemes require major modifications of AeroMACS. Even for the DF scheme, where the relay-aircraft is already able to perform all the decode-and-re-encode operations, multiple access, signaling and protocols currently considered in the WiMAX standard shall be modified to allow the user cooperation. These aspects represent a main drawback of cooperative schemes in the aeronautical framework. Some

cooperative schemes suffer also from a reduction of transmission efficiency. Considering a simple time-division scheme (as in our AF and DF implementation), where the transmission of the source and the one of the relay take place in two different time slots, the efficiency is reduced by a factor two. This is due to the fact that the transmission of a single message requires two time slots. Therefore, having assumed a code with rate R= 1/2 at the source, we obtain an overall rate of 1/4. Nevertheless, the efficiency reduction problem can be solved using coding cooperation schemes, which allow reaching rates up to 1/2 (that is the maximum for a system providing diversity two). Moreover, high rate scheme as the unequal diversity coding one [PUL12] [PUT12] [PUL12s] provides even higher rates (bigger than ½). This appealing result is achieved by scarifying a low-priority part of the message that obtains no diversity, while assuring diversity two to the high-priority segment of the message. The drawbacks of these techniques (i.e., the need of deep modification to the AeroMACS standard) put some limits to a rapid deployment of cooperative communications in the airport environment. However, the large benefits and great potential of these methods constitute an appealing solution for AeroMACS, especially under the light of future higher demand of reliability and capacity. Hence, this technique remains a valid solution for the (farer) long term evolution of AeroMACS.

5 Investigation on Potential Improvements of the Protocol

The AeroMACS profile is a modified sub-set of the WiMAX profile [WMF01], which is in turn only a sub-set of the actual IEE802.16 standard [WiM03]. This and the fact that the IEEE standard is very exhaustive indicate that an effective path of evolution of AeroMACS is the incorporation of already standardized protocols into the profile. This allows extending and optimizing the feature set provided by AeroMACS, while keeping the risks introduced by experimental technology to a minimum.

In addition, it may be possible to benefit from future developments of WiMAX. In particular, a new revision of the WiMAX profile (rel.1.5) has been defined and should be examined for adaptation to AeroMACS.

5.1 Network Re-Entry and Handover Optimization

Report [D31], to which the deliverables of this SP were used as input, identified handover optimization as one particular point of further research. Handover optimization is currently not included in the proposed AeroMACS profile [D32], however supporting it is included in the ranging-response message RNG-RSP ([WMF01] 6.3.2.3.6). Handover optimization allows certain management messages to be omitted during handover or network re-entry if MS and BS context information has already been obtained by other means (e.g. previous connection, backbone). In this case, the BS may decide to transmit unsolicited SS-basic-capability-response (SBC-RSP) and registration-response (REG-RSP) messages to the MS, making the handover/re-entry process shorter. To be more precise, the BS may indicate to the MS in the RNG-RSP message which handover/re-entry management messages may be omitted. The following messages may be omitted if the respective information is already present at the BS [D01]:

- Support Omission of SBC-REQ management messages.
- Support "Full State Sharing". No exchange of network re-entry messages after ranging before resuming normal operations
- Support SBC-RSP TLVs as part of RNG-RSP message. When the compound SBC-RSP encodings and REG-RSP encodings are included in RNG-RSP for HO optimization, the target BS shall only include TLV fields which values are different from what are used in the serving BS. For the TLV fields that are not included in the compound SBC-RSP and REG-RSP encodings, the MS shall set the values according to what are used in the serving BS
- Support Omission of REG-REQ during NW reentry. It is the registration request message
- Support REG-RSP TLV as part of RNG-RSP message. REG-RSP TLV items for HO optimization can be included in RNG-RSP TLV.
- OFDMA Fast Ranging IE. For the purpose of expediting NW re-entry of the MS with the target BS, the serving BS may negotiate with target BS allocation of a non-contention-based ranging opportunity for the MS, i.e., an unsolicited UL allocation for transmission of RNG-REQ message. A Fast_Ranging_IE may be placed in the UL-MAP message by a BS to provide a non-contention-based initial-ranging opportunity. The Fast_Ranging_IE shall be placed in the extended UIUC within a UL-MAP IE.
- Support sending Bandwidth Request header with zero Bandwidth Request as a notification of MS's successful reentry registration.
- Support sending at BS and receiving at MS traffic IP address refresh bit. The MS shall trigger a higher layer protocol required to refresh its traffic IP address.

Items identified for further investigation in [D01] are:

- Support Omission of PKM Authentication phase except TEK Phase. If security requirements allow for skipping authentication every time a handover takes place, then it shall be supported for overhead reduction.
- Support Omission of PKM TEK creation phase during re-entry processing. If security requirements allow for skipping key creation every time a handover takes place, then it shall be supported for overhead reduction.

Note that the AeroMACS profile is currently based on the WiMAX profile rel 1.0. The WiMAX profile has been updated to rel1.5 [WMF01]. It is recommended investigating newly added HO features esp. seamless handovers.

5.2 Multicast and Broadcast services

Currently, the multicast and broadcast services (MBS) of [WiM03] are not certified by WiMAX forum (i.e. are not part of any WiMAX profile). Consequently, commercial of the shelf products supporting MBS are not available and existing implementations may be considered experimental. [D32] proposes for AeroMACS to support multicast and broadcast, in order to set up multicast connections with shared connection identifiers CIDs. However, a standard conformant MBS would certainly be more desirable. It is recommended to re-investigate MBS certification when it is incorporated into an updated WiMAX profile release.

6 Summary

This report has been dedicated to the long term evolution of AeroMACS, and presented investigations of potential extensions, improvements, and general enhancements to the system baseline. Several aspect related to a potential future development of AeroMACS have been tackled, spanning from potential extensions of the use of the system, to investigations on potential enhancements of the waveform.

An investigation of the applicability of AeroMACS to the landing, take-off, and approach aircraft phases has been proposed. Numerical results showed good performance in correspondence of the new scenarios without degradation with respect to the taxi one (i.e. a classical airport aircraft phase). Moreover, the analysis of the synchronization algorithms illustrated good estimation accuracy in every considered scenario.

Passive radar functionality by means of AeroMACS signals as sources of opportunity has been investigated. The radar ambiguity function has been defined in order to estimate the spatial resolution as well as artefacts due to the synchronization pilot tones. The computation of the radar coverage of a single system has been performed, showing that the AeroMACS signal could represent a good candidate for short range passive radar applications.

A study of potential solutions for enhancing the performance of AeroMACS has been carried out. Since the performance of the system showed degradation in correspondence of the channel scenarios characterized by slow fading and lack of diversity, we investigated potential methods for increasing the diversity of the system, and thus improving its performance. We investigated techniques based on time diversity and spatial (cooperation) diversity as packet-level coding (in particular based on F-IRA codes) and cooperative communications (amplify and forward, decode and forward, unequal diversity coding), respectively.

All the investigated methods provide large performance gains, and hence, represent appealing solutions. Though, they require different modifications to the system base line, and in some cases imply drawbacks as efficiency reduction or increased delays. Focusing on the tradeoff between performance and costs, the packet-level coding method provides the best results. Indeed, this upgrade doesn't require hardware modifications, and brings large benefits to broadcast/multicast services. For the very long term AeroMACS evolution, more sophisticated methods might be accounted to answer potential higher demand of reliability and capacity. Hence, within this scenario, cooperative communications might represent appealing candidates (further investigations would be required in this framework).

An analysis of potential improvements of the protocol is included, together with an investigation on network re-entry and handover optimization. In particular, the adoption of features already included in the WiMAX standard, but not accounted by AeroMACS, is evaluated. The handover optimization might represent an interesting research theme. Indeed, this would allow omitting some management messages, and making the handover/re-entry process shorter.

References

SANDRA Internal Documentation

[D612] SANDRA D6.1.2 - Airport Data Link Requirements

[D621] SANDRA D6.2.1 – Report on Modeling and Performance Simulations

[D622] SANDRA D6.2.2 – AeroMACS Profile Recommendation Document

External Documentation

[WiM01] IEEE. Standard 802.16-2004. Part16: Air interface for fixed broadband wireless access systems, October 2004.

[WiM02] IEEE. Standard 802.16e-2005. Part16: Air interface for fixed and mobile broadband wireless access systems—Amendment for physical and medium access control layers for combined fixed and mobile operation in licensed band, December 2005.

[WiM03] IEEE Standard for Local and metropolitan area networks, Part 16: Air Interface for Broadband Wireless Access Systems, IEEE, 2009

[ICAO1] ICAO, http://aviationglossary.com

[D01] SESAR JU "AeroMACS Profile Analysis," Deliverable 15.02.07.D01 - T1.2/T1.3, 2012.

[D31] SESAR JU "AeroMACS Profile Evaluation and Validation," Deliverable 3.1, 2012.

[D32] SESAR JU "AeroMACS Profile Definition," Deliverable 3.2, 2012.

[WMF01] WiMAX Forum "WiMAX Forum Mobile System Profile Specification," rel. 1.5 Common Part, WMF-T23-001-R015v01, 2009.

[COCR] EUROCONTROL/FAA: Communications Operating Concept and Requirements for the Future Radio System, COCR Version 2.0.

[Gli09] S. Gligorevic, R. Zierhut, T. Jost, W. Wang, "Airport Channel Measurements at 5.2GHz", Proc. EUCAP-2009, March 2009.

[COV79] T. C. Cover, A. A. El Gamal, "Capacity theorems for the relay channel," IEEE Transaction on Information Theory, vol. IT-25, pp. 572–584, Sept. 1979.

[LAN01] J. N. Laneman, G. W. Wornell, and D. Tse, "An efficient protocol for realizingcooperative diversity in wireless network," in Proc. IEEE ISIT, Washington, DC, US, Jun. 2001, p. 294.

[SED03] A. Sedonaris, E.Erkip, B. Aazhang, "User Cooperation Diversity Part I," IEEE Transaction on Communications, vol. 51, no. 11, pp. 1927–48, Nov. 2003.

[SED03b] ——, "User Cooperation Diversity Part II," IEEE Transaction on Communications, vol. 51, no. 11, pp. 1927–48, Nov. 2003.

[LAN03] J. N. Laneman, G.W. Wornell, "Distributed space-time-coded protocols for exploiting cooperative diversity in wireless networks," IEEE Transaction on Information Theory, vol. 49, no. 10, pp. 2415–25, Oct. 2003.

[ZHA03] B. Zhao, M. C. Valenti, "Some new adaptive protocols for the wireless relay channel," in Proceedings Allerton Conference Commun., Monticello, IL, US, Oct. 2003.

[HUN02] T. H.Hunter, A. Nosratinia, "Cooperative diversity through coding," in Proceedings IEEE ISIT, Lousanne, Switzerland, Jul. 2002, p. 220.

[HUN06] ——, "Diversity through Coded Cooperation," IEEE Transaction On Wireless Communications, vol. 5, no. 2, Feb. 2006.

[LIV11a] G. Liva, P. Pulini, and M. Chiani, "Flexible On-line Construction of IRA Codes for Packet Erasure Correction with Application to Aeronautical Communications," in Proc. IEEE Int. Conf. on Communications, Kyoto, Japan, Jun. 2011.

[PUL10b] P. Pulini and M. Chiani, "Improving the Forward Link of the Future Airport Data Link by Space-Time Coding," in Proc. InOwO'10, Hamburg, Germany, Sep. 2010.

[PUL10a] P. Pulini, "Forward Link Performance Analysis for the Future IEEE 802.16-based Airport Data-Link," in Proc. IEEE Int. Conf. on Communications, Cape Town, South Africa, May 2010.

[PUL12] P. Pulini, G. Liva, M. Chiani, "," in Proc. IEEE Int. Conf. on Comm., Ottawa, Canada, June 2012.

[PUT12] P.Pulini, "Performance analysis and improvement for the future aeronautical mobile airport communications system (AeroMACS)", PhD Thesis, Bologna, Italy, May 2012.

[PUL12s] P. Pulini, G. Liva, and M. Chiani, "Unequal Diversity LDPC Codes for Relay Channels," IEEE Transaction on Communications, 2012, submitted.

[LIV11b] G. Liva, P. Pulini, and M. Chiani, "On-Line Construction of Irregular Repeat Accumulate Codes for Packet Erasure Channels," IEEE Transaction on Wireless Communications, submitted 2011, (in press).

[PUL11] P. Pulini and M. Chiani, "Improving the performance of AeroMACS by cooperative communications," in Proc. Digital Avionics System Conference, DASC 30th, Seattle, WG, US, October 2011.

[LUB97] M. Luby, M. Mitzenmacher, M. A. Shokrollahi, D. A. Spielman, and V. Stemann, "Practical loss-resilient codes," in Proc. 29th Symp. Theory Computing, 1997, pp. 150–159.

[SHO06] M. Shokrollahi, "Raptor codes," IEEE Transactions on Information Theory, vol. 52, no. 6, pp. 2551–2567, Jun. 2006.

[LUB06] M. Luby, M. Watson, T. Gasiba, T. Stockhammer, and W. Xu, "Raptor codes for reliable download delivery in wireless broadcast systems," in Proc. of IEEE Consumer Communications and Networking Conf., vol. 1, Jan. 2006, pp. 192–197.

[LIV10] G. Liva, E. Paolini, and M. Chiani, "Performance versus overhead for fountain codes over Fq," IEEE Comm. Letters., vol. 14, no. 2, pp. 178–180, 2010.

[BYE02] J. Byers, M. Luby, and M. Mitzenmacher, "A digital fountain approach to reliable distribution of bulk data," IEEE Journal on Selected Areas in Communications, vol. 20, no. 8, pp. 1528–1540, Oct. 2002.

[MET84] J. Metzner, "An improved broadcast retransmission protocol," IEEE Trans. Commun., vol. 32, no. 6, pp. 679 – 683, jun 1984.

[MAT09] B. Matuz, G. Liva, E. Paolini, and M. Chiani, "Pivoting Algorithms for Maximum Likelihood Decoding of LDPC Codes over Erasure Channels," in Proc. IEEE Globecomm, Honolulu, USA, Nov. 2009.

[FAR06] G. Faria, J. Henriksson, E. Stare, and P. Talmola, "DVB-H: Digital Broadcast Services to Handheld Devices," Proceedings of the IEEE, vol. 94, no. 1, pp. 194–209, Jan 2006.

[DVB07] "Framing structure, channel coding and modulation for Satellite Services to Handheld devices (SH) below 3GHz," Digital Video Broadcasting (DVB), Blue Book, 2007.

[3GPP05] 3GPP TS 26.346 V6.1.0, "Technical specification group services and system aspects; multimedia broadcast/multicast service; protocols and codecs," 3GPP, Tech Rep., Jun. 2005.

[CAL07] G. P. Calzolari, M. Chiani, F. Chiaraluce, R. Garello, and E. Paolini, "Channel coding for future space missions: New requirements and trends," Proc. IEEE, vol. 95, no. 11, pp. 2157–2170, Nov. 2007.

[DEC07] T. DeCola, H. Ernst, and M. Marchese, "Performance analysis of ccsds file delivery protocol and erasure coding techniques in deep space environments," Comput. Netw., v. 51, pp. 4032–4049, Oct. 2007.

[DEC11] T. De Cola, E. Paolini, G. Liva, and G. P. Calzolari, "Reliability Options for Data Communications in the Future Deep-Space Missions," Proc. IEEE, 2011.

[GAL63] R. Gallager, Low-Density Parity-Check Codes. Cambridge, MA: M.I.T. Press, 1963.

[JIN00] H. Jin, A. Khandekar, and R. McEliece, "Irregular repeat-accumulate codes," in Proc. Int. Symp. on Turbo codes and Related Topics, Sep. 2000, pp. 1–8.

[PAO08] E. Paolini, G. Liva, M. Varrella, B. Matuz, and M. Chiani, "Low-Complexity LDPC Codes with Near-Optimum Performance over the BEC," in Proc. 4th ASMS Conference, Bologna, August 2008.